RSC Advances

REVIEW

View Article Online
View Journal | View Issue

Cite this: *RSC Adv.*, 2015, **5**, 86219

Optical temperature sensing of rare-earth ion doped phosphors

Xiangfu Wang,*[ab] Qing Liu,[a] Yanyan Bu,[a] Chun-Sheng Liu,[ab] Tao Liu[a] and Xiaohong Yan*[abc]

Accurate and reliable temperature measurement of many special inaccessible objects is a challenging task. Optical temperature sensing is a promising method to achieve it. The current status of optical thermometry of rare-earth ion doped phosphors is reviewed in detail. Based on the mechanisms of optical temperature sensing of different phosphors, temperature dependent luminescence spectra, the fluorescence intensity ratio technique in the data fitting process, and errors of the energy difference between thermally coupled levels, we describe the recent developments in the use of optical thermometry materials. The most important results obtained in each case are summarized, and the main challenges that we need to overcome are discussed. Research in the field of phosphor sensors has shown that they have significant advantages compared to conventional sensors in terms of their properties like greater sensitivity, freedom from electromagnetic interference, long path monitoring, and independence of compatibility with electronic devices.

Received 22nd August 2015
Accepted 28th September 2015

DOI: 10.1039/c5ra16986k

www.rsc.org/advances

1. Introduction

Temperature is a key parameter to induce some changes of cellular events, physical and chemical properties of functional nanomaterials, functional degradation of microcircuits, and so on. Contact temperature measurement, just like a thermometer, is an ideal method to study some phenomena that change with temperature. However, especially at the submicron scale, for temperature fluctuations of microcircuits and intracellular liquids, the conventional thermometer is not able to make measurements.[1–3] Brites and Jaque reported some examples of luminescent and non-luminescent thermometers working at the nanometric scale.[4,5] Even so, it is difficult to measure directly the temperatures of inaccessible objects, such as high-voltage power stations, coal mines, and volcanic and corrosive circumstances.[6–9] Therefore, the ability to glean the temperature of the above objects could have valuable repercussions leading to novel insight about their properties induced by a temperature change.

[a]College of Electronic Science and Engineering, Nanjing University of Posts and Telecommunications, Nanjing, 210046, People's Republic of China. E-mail: xfwang@njupt.edu.cn; yanxh@njupt.edu.cn
[b]Key Laboratory of Radio Frequency and Micro-Nano Electronics of Jiangsu Province, Nanjing 210046, Jiangsu, China
[c]College of Science, Nanjing University of Aeronautics and Astronautics, Nanjing 210046, People's Republic of China

Xiangfu Wang received his PhD degree from Nanjing University of Aeronautics and Astronautics, in 2012. From 2012 to present, he was promoted to an associate professor in the College of Electronic Science and Engineering at Nanjing University of Posts and Telecommunications. His current research concentrates on the synthesis, growth mechanism, photoluminescence and optical temperature sensing of rare-earth ion doped nanomaterials and transparent glass ceramics.

Qing Liu obtained her Bachelor degree from Nanjing University of Posts and Telecommunications, in 2015. From 2015 to present, she works for a Master degree in Xiangfu Wang's group. Her current research concentrates on the photoluminescence of rare-earth ion doped nanomaterials.

Optical temperature sensing, in contrast to other thermometers, is a promising method to achieve contactless measurement and large-scale imaging. Optical temperature sensing is based on monitoring the emission intensity change of luminescent materials induced by temperature when they interact with physical systems. Phosphors with an intense emission intensity are used as temperature detectors to convert the measured spectrum to temperature. It is easy to calibrate and calculate the temperature change range only through the main parameters of luminescence including intensity, effective bandwidth, spectrum shape, spectral shift and lifetime.

Recently, CdSe and CdTe semiconducting quantum dots were used as optical temperature nanoprobes in the low temperature range, since the peak position of the emission wavelength changes as a function of temperature.[10,11] Organic compounds, such as Rhodamine B, the Ru–phen complex, DPTB dissolved in MOE, and so on, were used for dye-based intensity luminescence nanothermometry, due to their the spectral properties depending on many factors, such as the solvent, concentration, pH and temperature.[5,11,12] These quantum dot nanocrystals and organic compounds are easily oxidized at high temperature, and are only available in the low temperature range. To overcome this, rare-earth ion doped oxide crystals, glass, core–shell heterojunction nanoparticles, and transparent glass ceramics containing fluoride nanocrystals were fabricated and used as optical temperature sensors. The present review aims to describe the latest progress of optical thermometry based on the luminescence of rare-earth ion doped phosphors. It contains fundamental principles, different rare-earth ion doped phosphors for optical thermometry, a conclusion and the main challenges.

2. Fundamental principles of optical temperature sensing

Phosphor thermometry is a non-contact technique that uses luminescence signals to measure temperature remotely. As shown in Fig. 1, phosphors are composed of a host and some luminescent ions, and will emit visible, infrared, or ultraviolet radiation upon excitation from an external light source. The intensity, wavelength, and lifetime of the emission bands are used to determine the temperature of a surface. Thus, the choice of luminescent ions is important to measure the temperature change around phosphors. Among the metal ions

Yanyan Bu obtained her Master degree from Xiangtan University, in 2010. From 2010 to present, she works in Nanjing University of Posts and Telecommunications. From 2014 to present, she works for a Doctor degree in Xiaohong Yan's group. Her current research concentrates on optical temperature sensing of rare-earth ion doped transparent glass ceramics.

Tao Liu obtained his Bachelor degree from Nanjing University of Posts and Telecommunications (NJUPT), China, in 2012, and he received his M.S degree from NJUPT in 2015 under the supervision of Prof. Xiaohong Yan and Prof. Xiangfu Wang. His current research concentrates on Computer Graphics.

Chun-Sheng Liu received his PhD in 2011 from Institute of Solid State Physics, Chinese Academy of Sciences. Then he was awarded an AvH (Alexander von Humboldt Foundation) Fellowship (2011–2013) in Technische Universitaet München, Germany. In 2014, he was promoted to a full professor in the College of Electronic Science and Engineering at Nanjing University of Posts and Telecommunications (NJUPT). He was elected as Specially-Appointed Professors by NJUPT in Jiangsu Province. His main research fields are functional materials for hydrogen storage, gas sensors, and photocatalysis.

Xiaohong Yan received his PhD degree from Institute of Solid State Physics, Chinese Academy of Science, in 1997. From 2010 to present, he works as a full professor in the College of Electronic Science and Engineering at Nanjing University of Posts and Telecommunications. His current research concentrates on transport and manipulation of quantum systems and new energy materials.

used as luminescence centers, the trivalent rare-earth ions are especially attractive, due to abundant energy levels located at a wide wavelength range from ultraviolet to infrared.[13] Possessing real intermediate energy levels, trivalent rare-earth ions can give out desired emissions *via* various energies, due to abundant energy levels of 4f configurations. Inheriting their native intra-configurational transitions, trivalent rare-earth ion activated luminescent materials have received consistent attention due to large Stokes/anti-Stokes shifts, long luminescence lifetimes, and sharp band emissions.[14] Additionally, some trivalent rare-earth ions own a couple of adjacent levels with a very small energy gap (ΔE) of about 100–2000 cm^{-1}, such as Er^{3+}: $^2H_{11/2}$ and $^4S_{3/2}$; Tm^{3+}: $^3F_{2,3}$ and $^3H_4$; Ho^{3+}: $^5S_2$ and $^5F_4$; Nd^{3+}: $^4F_{5/2}$ and $^4F_{3/2}$; Dy^{3+}: $^4I_{15/2}$ and $^4F_{9/2}$; Eu^{3+}: $^5D_1$ and $^5D_0$, and so on. As shown in Fig. 1, in the photoluminescence process, these adjacent energy levels, the upper level and lower level, can be thermally populated and depopulated through changing the environmental temperature around the phosphors. The two adjacent energy levels were called thermally coupled energy levels (TCL). The luminescence intensity ratio between I_U and I_L will change regularly with the temperature increase. A function relation between the luminescence intensity ratio and temperature can be determined through fitting some data points at different temperatures.

The luminescence intensity of an emission band can be expressed as:

$$I_{ij} = hvA_{ij}N_i \quad (1)$$

where hv is the transition energy per photon from an i state to a j state, A_{ij} is the spontaneous radiative emission probability, and N_i is the state population of the i state.[15]

The term v is expressed as:

$$v = \frac{c}{\lambda} \quad (2)$$

where λ is the mean wavelength of the transition, $h$is Planck's constant, and c is the speed of light.

In conclusion, I_{ij} can be expressed as:

$$I_{ij} = \frac{hc}{\lambda}A_{ij}N_i \quad (3)$$

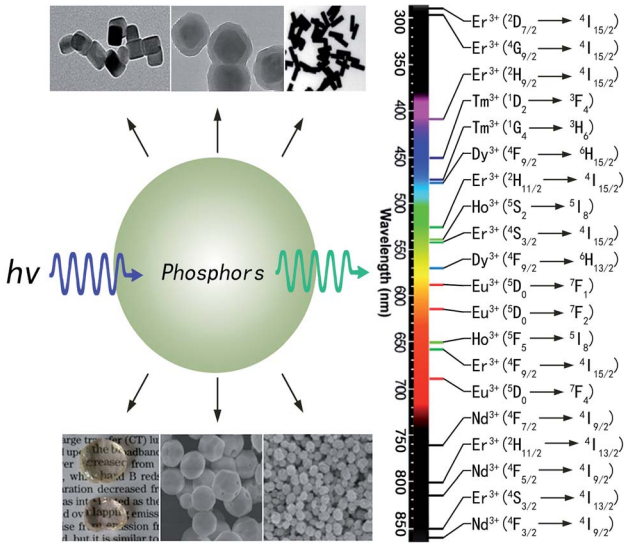

Fig. 2 Different types and luminescence transitions of rare-earth ion doped phosphors used for optical thermometry. Data are summarized according to ref. 21–80.

The ratio of the luminescence from each thermally coupled level of active ions is modified as:

$$R = \frac{I_U}{I_L} \quad (4)$$

where I_U and I_L are the fluorescence intensities generated by the radiative transitions from the upper and lower thermally coupled levels to the ground level.

Thus, the term R can be given as the following:

$$R = \frac{\lambda_L A_{Uj} N_U}{\lambda_U A_{Lj} N_L} \quad (5)$$

where λ_L is the mean wavelength of the L → j transition, λ_U is the mean wavelength of the U → j transition, A_{Uj} is the spontaneous radiative emission probability of the U → j transition, and A_{Lj} is the spontaneous radiative emission probability of the L → j transition. N_U and N_L are the state populations of the upper and lower levels.

The terms A_{Uj}, A_{Lj}, N_U, and N_L are dependent on the temperature. The population process of the N_U and N_L levels

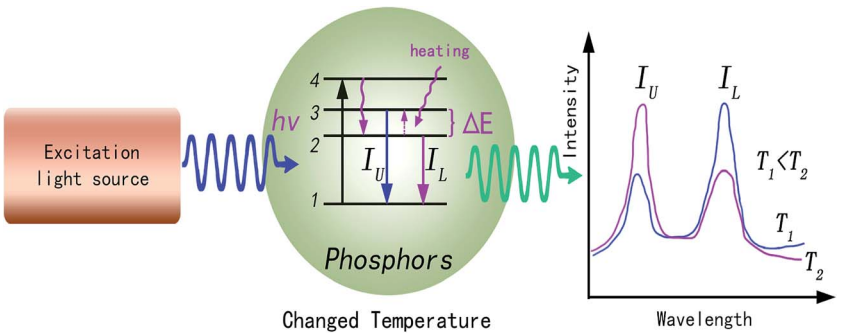

Fig. 1 Schematic illustration of the basic mechanism of the optical thermometry process in rare-earth ion doped phosphors.

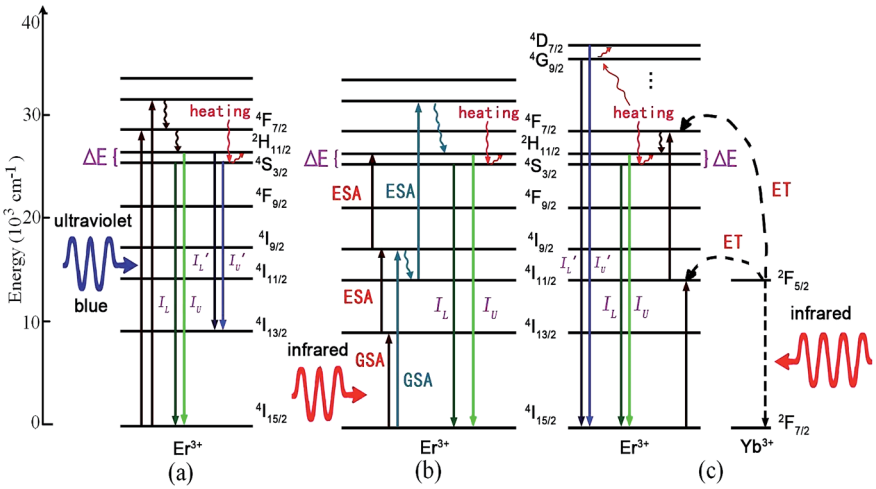

Fig. 3 The mechanism of optical thermal sensing through (a) Er^{3+} down-conversion under ultraviolet (blue) excitation, (b) Er^{3+} up-conversion under infrared excitation, and (c) Yb^{3+}–Er^{3+} energy transfer under infrared excitation.

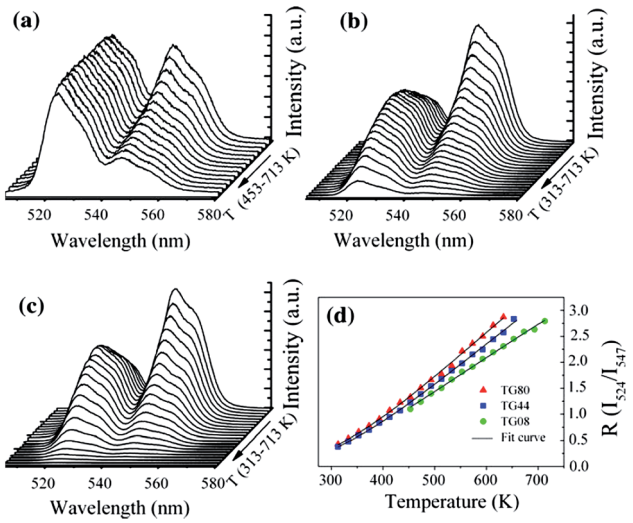

Fig. 4 Temperature dependent Er^{3+} green emission spectra of 0.5 mol% Er^{3+} doped (a) $Te_{80}Zn_{9.5}Na_{10}$ (TG08) glass, (b) $Te_{40}Ge_{40}Zn_{9.5}Na_{10}$ (TG44) glass, (c) $Ge_{80}Zn_{9.5}Na_{10}$ (TG80) glass, and (d) temperature dependent R values of the two green emissions of Er^{3+}. Reprinted from ref. 21 with permission of Springer.

obeys the Boltzmann distributing law.[16] Thus, R can be expressed as:

$$R = A \exp\left[\frac{-\Delta E_f}{KT}\right] + B \quad (6)$$

where A is a fitting constant that depends on the experimental system and intrinsic spectroscopic parameters; ΔE_f is the fitting energy difference between thermally coupled levels; K is the Boltzmann constant (298 K, $KT \approx 210$ cm^{-1}); T is the absolute temperature; and B is an offset.[17,18] The term B includes the overlapping of fluorescence peaks originating from the two individual thermally coupled energy levels, and stray light originating from other energy levels or from the excitation. B is expressed as:

$$B = \frac{m}{n} \quad (7)$$

where n defines the fraction of the total fluorescence intensity, and m defines the fraction of the total intensity.

The sensitivity is a key parameter to value the possibility of practical applications. The sensitivity of optical thermometry is the rate of change of R in response to the variation of temperature.[17,19,20] To allow comparison between the sensitivities obtained from different thermally coupled levels, the relative sensitivity S_R and the absolute sensitivity S_A are defined as:

$$S_R = \frac{dR}{dT} = R\frac{\Delta E_f}{KT^2} \quad (8)$$

and

$$S_A = \frac{1}{R}\frac{dR}{dT} = \frac{\Delta E_f}{KT^2} \quad (9)$$

where ΔE_f is the fitting energy difference between thermally coupled levels.

The terms S_R and S_A are dependent on ΔE_f. If ΔE_f agrees well with the experimental energy difference ΔE_m, the values of S_R and S_A are accurate. The error δ between ΔE_f and ΔE_m is expressed as:

$$\delta = \frac{|\Delta E_f - \Delta E_m|}{\Delta E_m} \quad (10)$$

where ΔE_m is calculated from the two analyzed peaks in the spectrum. The error δ is a key parameter to determine whether the value of ΔE_f agrees well with the experimental value of ΔE_m. A large value of δ means that the energy transfer between thermally coupled levels and other levels is not neglected, and the population of thermally coupled levels at high temperature is induced by the routes of the Boltzmann distribution and energy transfer.[4,14,17]

Table 1 The maximum sensitivity values of Er^{3+} doped phosphors by the fluorescence intensity ratio technique are presented, and the involved transitions from the TCL, excition wavelength, emission wavelength, and temperature range are included

Rare-earth ions	Host	λ_{ex} (nm)	λ_{em} (nm)	Transitions	Temperature range (K)	S_R (maximum)	S_A	Ref.
Er^{3+}	Tellurite glass	379	524, 547	$^2H_{11/2}$, $^4S_{3/2} \rightarrow {}^4I_{15/2}$	313–713	0.0085 K^{-1} (596 K)	$1108.3/T^2$	21
Er^{3+}	In–Zn–Sr–Ba glass	406	523, 545	$^2H_{11/2}$, $^4S_{3/2} \rightarrow {}^4I_{15/2}$	125–425	0.0028 K^{-1} (425 K)	$1167.6/T^2$	22
Er^{3+}	α-$NaYF_4$ glass ceramics	488	525, 550	$^2H_{11/2}$, $^4S_{3/2} \rightarrow {}^4I_{15/2}$	300–720	0.0024 K^{-1} (540 K)	$1051.51/T^2$	23
Er^{3+}	PKAZLF glass	488	524, 550	$^2H_{11/2}$, $^4S_{3/2} \rightarrow {}^4I_{15/2}$	298–773	0.0079 K^{-1} (630 K)	$1238.8/T^2$	24
Er^{3+}	Te–Pb–Al glass	488	530, 550	$^2H_{11/2}$, $^4S_{3/2} \rightarrow {}^4I_{15/2}$	100–573	0.0079 K^{-1} (541 K)	$1149.43/T^2$	25
Er^{3+}	Sr–Ba–Nb–B glass	532	800, 850	$^2H_{11/2}$, $^4S_{3/2} \rightarrow {}^4I_{13/2}$	300–700	0.0017 K^{-1} (600 K)	$1255.14/T^2$	26
Er^{3+}	Te–Pb–Al glass	800	530, 550	$^2H_{11/2}$, $^4S_{3/2} \rightarrow {}^4I_{15/2}$	300–550	0.0054 K^{-1} (540 K)	$1085.57/T^2$	27
Er^{3+}	ZBLALiP glass	805	522, 546	$^2H_{11/2}$, $^4S_{3/2} \rightarrow {}^4I_{15/2}$	150–850	0.0023 K^{-1} (495 K)	$981/T^2$	28
Er^{3+}	Ba(Zr,Ca)TiO_3 ceramics	980	525, 550	$^2H_{11/2}$, $^4S_{3/2} \rightarrow {}^4I_{15/2}$	200–443	0.0044 K^{-1} (443 K)	$1135.5/T^2$	29
Er^{3+}	Si–B–Ba–Na glass	978	534, 549	$^2H_{11/2}$, $^4S_{3/2} \rightarrow {}^4I_{15/2}$	296–673	0.0023 K^{-1} (296 K)	$335/T^2$	30
Er^{3+}	$BaTiO_3$ nanocrystals	980	526, 547	$^2H_{11/2}$, $^4S_{3/2} \rightarrow {}^4I_{15/2}$	322–466	1200 K^{-1}	$940/T^2$	31
Er^{3+}	PLZT ceramics	980	534, 565	$^2H_{11/2}$, $^4S_{3/2} \rightarrow {}^4I_{15/2}$	310–883	0.004 $°C^{-1}$ (610 °C)	$1096.92/T^2$	32
Er^{3+}, Mo^{6+}	YbAG	976	522, 546	$^2H_{11/2}$, $^4S_{3/2} \rightarrow {}^4I_{15/2}$	295–973	0.0048 K^{-1} (467 K)	$900.8/T^2$	33
Er^{3+}	ZnO	978	536, 553	$^2H_{11/2}$, $^4S_{3/2} \rightarrow {}^4I_{15/2}$	353–973	0.0062 $°C^{-1}$ (170 °C)	$880.11/T^2$	34
Er^{3+}	Chalcogenide glass	1540	530, 555	$^2H_{11/2}$, $^4S_{3/2} \rightarrow {}^4I_{15/2}$	293–493	0.0102 $°C^{-1}$	$1135.23/T^2$	35
Er^{3+}	$Na_{0.82}Ca_{0.08}Er_{0.16}Y_{0.853}F_4$	1540	523, 542	$^2H_{11/2}$, $^4S_{3/2} \rightarrow {}^4I_{15/2}$	5–300	0.0022 K^{-1} (338 K)	$958.28/T^2$	36
Er^{3+}, Yb^{3+}	α-$NaYF_4$	980	525, 545	$^2H_{11/2}$, $^4S_{3/2} \rightarrow {}^4I_{15/2}$	298–318	0.0030 K^{-1} (515 K)	$1028/T^2$	37
Er^{3+}, Yb^{3+}	β-$NaLuF_4$	980	256, 276	$^4D_{7/2}$, $^4G_{9/2} \rightarrow {}^4I_{15/2}$	303–523	0.0052 K^{-1} (303 K)	$384/T^2$	38
Er^{3+}, Yb^{3+}, Eu^{3+}	Y_2O_3	980	523, 551	$^2H_{11/2}$, $^4S_{3/2} \rightarrow {}^4I_{15/2}$	303–593	0.0103 K^{-1} (593 K)	$1062.50/T^2$	39
Er^{3+}, Yb^{3+}	Y_2O_3	978	539, 564	$^2H_{11/2}$, $^4S_{3/2} \rightarrow {}^4I_{15/2}$	150–300	0.0528 K^{-1} (150 K)	$1173.39/T^2$	40
Er^{3+}, Yb^{3+}	Y_2O_3	980	528, 556	$^2H_{11/2}$, $^4S_{3/2} \rightarrow {}^4I_{15/2}$	93–613	0.0044 K^{-1} (427 K)	$886.08/T^2$	41
Er^{3+}, Yb^{3+}, Eu^{3+}	Y_2O_3	980	523, 551	$^2H_{11/2}$, $^4S_{3/2} \rightarrow {}^4I_{15/2}$	301–403	0.0008 K^{-1} (327 K)	$682.6/T^2$	42
Er^{3+}, Yb^{3+}	Al_2O_3	978	523, 545	$^2H_{11/2}$, $^4S_{3/2} \rightarrow {}^4I_{15/2}$	295–973	0.0051 K^{-1} (495 K)	$964.1/T^2$	43
Er^{3+}, Yb^{3+}	$BaMoO_4$	980	531, 552	$^2H_{11/2}$, $^4S_{3/2} \rightarrow {}^4I_{15/2}$	303–523	0.0206 K^{-1} (463 K)	$873.38/T^2$	44
Er^{3+}, Yb^{3+}	Y_2SiO_5 pulsed	975	530, 550	$^2H_{11/2}$, $^4S_{3/2} \rightarrow {}^4I_{15/2}$	300–600	0.0070 K^{-1} (600 K)	$1226/T^2$	45
Er^{3+}, Yb^{3+}, Nd^{3+}	Y_2SiO_5	808	528, 556	$^2H_{11/2}$, $^4S_{3/2} \rightarrow {}^4I_{15/2}$	298–753	0.00095 K^{-1}(439 K)	$710.87/T^2$	46
Er^{3+}, Yb^{3+}	$SrWO_4$	980	525, 547	$^2H_{11/2}$, $^4S_{3/2} \rightarrow {}^4I_{15/2}$	300–518	0.01498 K^{-1} (403 K)	$866.17/T^2$	47
Er^{3+}, Yb^{3+}	YVO_4	980	524, 554	$^2H_{11/2}$, $^4S_{3/2} \rightarrow {}^4I_{15/2}$	300–485	0.01169 K^{-1} (380 K)	$774.1/T^2$	48
Er^{3+}, Yb^{3+}	$CaWO_4$	980	384, 408	$^4G_{11/2}$, $^2H_{9/2} \rightarrow {}^4I_{15/2}$	303–873	0.0073 K^{-1} (873 K)	$2109.31/T^2$	51
Er^{3+}, Mo^{6+}	$Yb_2Ti_2O_7$	976	532, 546	$^2H_{11/2}$, $^4S_{3/2} \rightarrow {}^4I_{15/2}$	290–610	0.0074 K^{-1} (340 K)	$679.2/T^2$	52
Er^{3+}, Yb^{3+}	$LiNbO_3$	980	530, 550	$^2H_{11/2}$, $^4S_{3/2} \rightarrow {}^4I_{15/2}$	285–453	0.0075 K^{-1} (310 K)	$1250/T^2$	54
Er^{3+}, Yb^{3+}	$Na_{0.5}Bi_{0.5}TiO_3$ ceramics	980	525, 550	$^2H_{11/2}$, $^4S_{3/2} \rightarrow {}^4I_{15/2}$	173–553	0.0035 K^{-1} (493 K)	$1017.12/T^2$	49
Er^{3+}, Yb^{3+}	$NaBiTiO_3$ ceramics	980	525, 550	$^2H_{11/2}$, $^4S_{3/2} \rightarrow {}^4I_{15/2}$	163–613	0.0031 K^{-1} (400 K)	$827.26/T^2$	50
Er^{3+}, Yb^{3+}	$Bi_7Ti_4NbO_{21}$	980	547, 670	$^4S_{3/2}$, $^4F_{9/2} \rightarrow {}^4I_{15/2}$	153–553	0.0044 K^{-1}		53
Er^{3+}, Yb^{3+}	TeO_2–WO_3 glass	980	527, 551	$^2H_{11/2}$, $^4S_{3/2} \rightarrow {}^4I_{15/2}$	300–690	0.0029 K^{-1} (690 K)	$976.75/T^2$	55

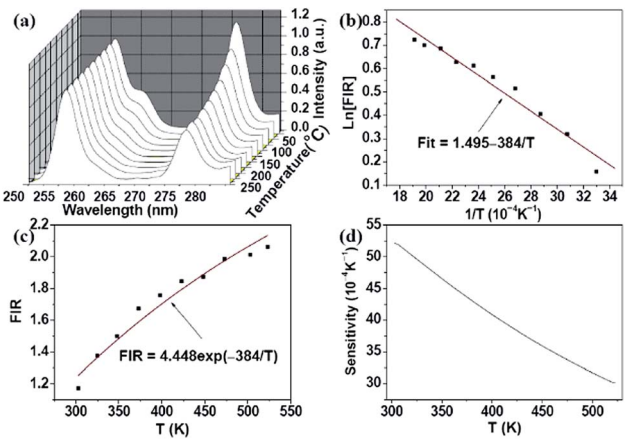

Fig. 5 Temperature dependent (a) spectrum of Er^{3+} ions from $^4D_{7/2}$ and $^4G_{9/2}$ levels; (b) log plot of the FIR; (c) FIR relative to the temperature; and (d) sensor sensitivity under 980 nm excitation. Reprinted from ref. 38 with permission of Optical Society of America.

3. Rare-earth ion doped phosphors for optical thermometry

Phosphors are composed of inorganic oxides and ceramic materials which means that phosphors are resistant to oxidation in high temperature environments and are non-reactive with harsh chemicals. To obtain excellent optical temperature sensors, trivalent lanthanide ion doped phosphors were synthesized widely.[21–80] At present, trivalent lanthanide ions, such as Er^{3+}, Tm^{3+}, Ho^{3+}, Nd^{3+}, Dy^{3+}, and Eu^{3+}, have been used as luminescence centers (or activators) in the process of optical thermometry, as shown in Fig. 2. Host materials used for optical thermometry involve nanorods,[60] spherical and tetragonal nanoparticles,[59] core–shell particles,[61] hollow nanoparticles, glass ceramics containing fluoride nanocrystals,[23,68,71] fibers,[17] and oxide bulks.[34,39–54,58] Phosphors are excited with a light source, and the emitted luminescence can be in the ultraviolet, visible, or even in the infrared region.

For optical temperature sensors, the TCL should satisfy some conditions that depend strongly on the host matrix into

Table 2 Host dependent ΔE_f, ΔE_m, and δ in Er^{3+} doped and Yb^{3+}–Er^{3+} co-doped phosphors

Samples	ΔE_f (cm^{-1})	ΔE_m (cm^{-1})	δ (%)	Ref.
Er^{3+} doped tellurite glass	781	802	2.62	21
Er^{3+} doped In–Zn–Sr–Ba glass	861	771.8	11.55	22
Er^{3+} doped α-$NaYF_4$ glass ceramics	741	865.8	14.41	23
Er^{3+} doped PKAZLF glass	873	902.2	3.24	24
Er^{3+} doped Te–Pb–Al glass	810	686	18.1	25
Er^{3+} doped Sr–Ba–Nb–B glass	872.3	748	16.62	26
Er^{3+} doped Te–Pb–Al glass	765	810	5.56	27
Er^{3+} doped ZBLALiP glass	681	700	2.72	28
Er^{3+} doped Ba(Zr,Ca)TiO_3 ceramics	789	850	7.18	29
Er^{3+} doped Si–B–Ba–Na glass	236	511.7	53.89	30
Er^{3+} doped $BaTiO_3$ nanocrystals	662.4	729.9	9.25	31
Er^{3+} doped PLZT ceramics	773	1027.5	24.77	32
Er^{3+}, Mo^{6+} co-doped YbAG	634.8	842.1	24.62	33
Er^{3+} doped ZnO	611	573.5	6.54	34
Er^{3+} doped chalcogenide glass	800	849.9	5.87	35
$Na_{0.82}Ca_{0.08}Er_{0.16}Y_{0.853}F_4$	675.3	670.27	0.75	36
Er^{3+}, Yb^{3+} co-doped α-$NaYF_4$	724.4	766.1	5.44	37
Er^{3+}, Yb^{3+} co-doped β-$NaLuF_4$	270.6	2830.6	90.44	38
Er^{3+}, Yb^{3+}, Eu^{3+} tri-doped Y_2O_3	738.54	800	7.68	39
Er^{3+}, Yb^{3+} co-doped Y_2O_3	826.9	810.6	2.01	40
Er^{3+}, Yb^{3+} co-doped Y_2O_3	615.7	800	23.0	41
Er^{3+}, Yb^{3+}, Eu^{3+} tri-doped Y_2O_3	474.9	971	51.09	42
Er^{3+}, Yb^{3+} co-doped Al_2O_3	679.4	771.8	11.97	43
Er^{3+}, Yb^{3+} co-doped $BaMoO_4$	607	716	15.22	44
Er^{3+}, Yb^{3+} co-doped Y_2SiO_5	781	686.1	13.83	45
Er^{3+}, Yb^{3+}, Nd^{3+} tri-doped Y_2SiO_5	498	601.7	17.23	46
Er^{3+}, Yb^{3+} co-doped $SrWO_4$	602	766.1	21.42	47
Er^{3+}, Yb^{3+} co-doped YVO_4	538	693	22.36	48
Er^{3+}, Yb^{3+} co-doped $Na_{0.5}Bi_{0.5}TiO_3$	706.8	800	11.65	49
Er^{3+}, Yb^{3+} co-doped $NaBiTiO_3$	574.8	800	28.15	50
Er^{3+}, Yb^{3+} co-doped $CaWO_4$	1455	1530	4.90	51
Er^{3+}, Mo^{6+} co-doped $Yb_2Ti_2O_7$	478.6	482	0.71	52
Er^{3+}, Yb^{3+} co-doped $Bi_7Ti_4NbO_{21}$	775	820.7	5.57	53
Er^{3+}, Yb^{3+} co-doped $LiNbO_3$	860	686.2	25.33	54
Er^{3+}, Yb^{3+} co-doped TeO_2–WO_3 glass	678.94	826.5	17.85	55

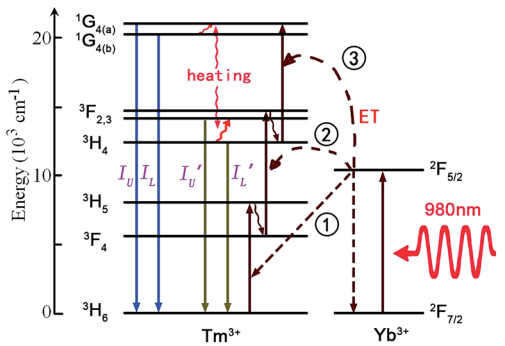

Fig. 6 The mechanism of optical thermal sensing through Yb^{3+}–Tm^{3+} energy transfer under 980 nm infrared excitation.

which the rare-earth ions are doped. The factors affecting the TCL of the rare-earth ions are as follows:

1. The separation between the TCL should be more than 200 cm^{-1} to avoid strong overlapping of the two fluorescence wavelengths, and be less than 2000 cm^{-1} to avoid too small a population in the upper level for the temperature range of interest.

2. In order to achieve a sufficient fluorescence intensity from the upper level transition, the radiative transitions from the upper level should dominate its non-radiative transitions.

TCL proven by experiment are listed as follows: Er^{3+}: $^2H_{11/2}$/$^4S_{3/2}$, and $^4D_{7/2}$/$^4G_{9/2}$; Tm^{3+}: $^3F_{2,3}$/$^3H_4$, and $^1G_{4(a)}$/$^1G_{4(b)}$; Ho^{3+}: $^5S_2$/$^5F_4$, $^5F_{2,3}$/$^3K_8$, and $^5G_6$/$^5F_1$; Nd^{3+}: $^4F_{5/2}$/$^4F_{3/2}$, $^4F_{7/2}$/$^4F_{3/2}$, and $^4F_{7/2}$/$^4F_{5/2}$; Dy^{3+}: $^4I_{5/2}$ and $^4F_{9/2}$; and Eu^{3+}: $^5D_1$/$^5D_0$. The TCL are populated by the up-conversion and down-conversion processes of the above trivalent rare-earth ions. Optical thermometry has been achieved by analyzing the temperature dependent luminescence properties originating from the transitions from the TCL to the other levels.

3.1 Optical thermometry based on Er^{3+} doped phosphors

Trivalent erbium Er^{3+} has a $4f^{11}$ electronic configuration and dense energy levels located at a wide wavelength range from ultraviolet to infrared, which is suitable to absorb and emit ultraviolet, visible and infrared luminescence. The Er^{3+} ion has two couples of adjacent TCL, $^2H_{11/2}$ and $^4S_{3/2}$, and $^4D_{7/2}$ and $^4G_{9/2}$, whose relative emission intensities are strongly temperature dependent. Among the different rare-earth ions capable of single-center phosphors, Er^{3+} is probably the most used one,

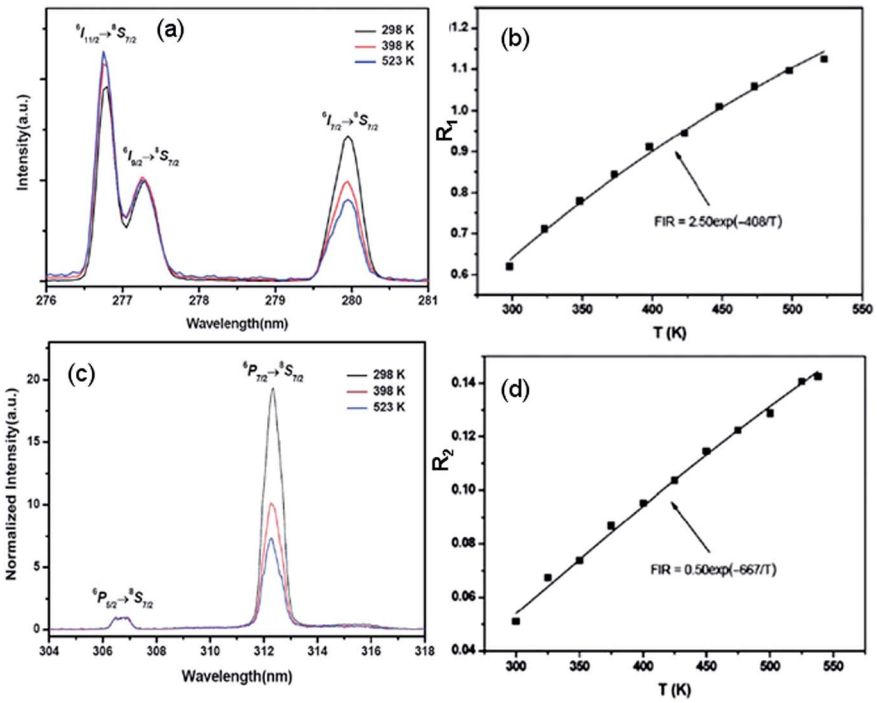

Fig. 7 Temperature dependent (a) ultraviolet spectra in the range of 276–281 nm, and (b) R_1 of the emissions from the transitions of $^6I_{9/2}/^8S_{7/2}$ and $^6I_{7/2}/^8S_{7/2}$ of NaLuF4:Yb^{3+}, Tm^{3+}, Gd^{3+} microcrystals. Temperature dependent (c) ultraviolet spectra in the range of 304–318 nm, and (d) R_2 of the emissions from the transitions of $^6P_{5/2}/^8S_{7/2}$ and $^6P_{7/2}/^8S_{7/2}$ of $NaLuF_4$:Yb^{3+}, Tm^{3+}, Gd^{3+} microcrystals. Reproduced from ref. 60 with permission of the Royal Society of Chemistry.

due to its very intense two green emission bands originating from the $^2H_{11/2}$ and $^4S_{3/2}$ TCL. As shown in Fig. 3, the mechanism of optical thermometry based on Er^{3+} doped phosphors can be summarized as follows:

(1) Down-conversion of Er^{3+} ions under ultraviolet (or blue) excitation:[21–26] under ultraviolet (or blue) excitation, Er^{3+} ions are excited directly to the higher excited states by ground state absorption (GSA), as shown in Fig. 3(a). Some ions in the excited states relax to the next lower energy levels $^2H_{11/2}$ and $^4S_{3/2}$ through the process of non-radiative relaxation, making the $^2H_{11/2}$ and $^4S_{3/2}$ levels populated. Er^{3+} ions in the $^2H_{11/2}$ and $^4S_{3/2}$ levels radiatively relax to the $^4I_{15/2}$ level, giving two green emissions with the intensity of I_U and I_L. Er^{3+} ions in the $^2H_{11/2}$ and $^4S_{3/2}$ levels radiatively relax to the $^4I_{13/2}$ level, giving two green emission bands with the intensity of I'_U and I'_L. The

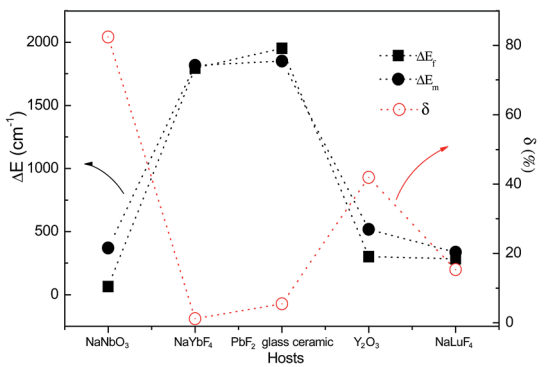

Fig. 8 Host dependent ΔE_f and ΔE_m between the TCL of Tm^{3+} ions, and the corresponding δ values.

Table 3 The maximum sensitivity values of Tm^{3+} doped phosphors by the fluorescence intensity ratio technique are presented, and the involved transitions from the TCL, excition wavelength, emission wavelength, and temperature range are included

Rare-earth ions	Host	λ_{ex} (nm)	λ_{em} (nm)	Transitions	Temperature range (K)	S_R (maximum)	S_A	Ref.
Tm^{3+}, Yb^{3+}	$NaNbO_3$	976	480, 486	$^1G_4$, $^3F_{2,3}$, $^3H_4 \rightarrow {}^3H_6$	293–353	0.0008 $°C^{-1}$ (25 °C)	$93.53/T^2$	56
Tm^{3+}, Yb^{3+}	PbF_2 glass ceramics	980	700, 800	$^3F_{2,3}$, $^3H_4 \rightarrow {}^3H_6$	293–703	0.0006 K^{-1} (1360 K)	$2829.5/T^2$	57
Tm^{3+}, Yb^{3+}	Y_2O_3	976	476, 488	$^1G_{4(a)}$, $^1G_{4(b)} \rightarrow {}^3H_6$	303–753	0.0035 K^{-1} (303 K)	$452.51/T^2$	58
Tm^{3+}, Yb^{3+}	Y_2O_3	978	454, 815	$^1D_2 \rightarrow {}^3F_4$, $^3H_4 \rightarrow {}^3H_6$	10–300	0.078 K^{-1} (270 K)	$566.91/T^2$	59
Tm^{3+}, Yb^{3+}, Gd^{3+}	$NaLuF_4$	980	307, 312.4	$^6P_{5/2}$, $^6P_{7/2} \rightarrow {}^8S_{7/2}$	298–523	0.0004 K^{-1} (333 K)	$667/T^2$	60
		980	277.3, 279.9	$^6I_{9/2}$, $^6I_{7/2} \rightarrow {}^8S_{7/2}$	298–523	0.0029 K^{-1} (298 K)	$408/T^{-2}$	60
Tm^{3+}	$NaYbF_4$@SiO_2	980	697, 798	$^3F_{2,3}$, $^3H_4 \rightarrow {}^3H_6$	100–700	0.00054 K^{-1} (100 K)	$2677.39/T^2$	61

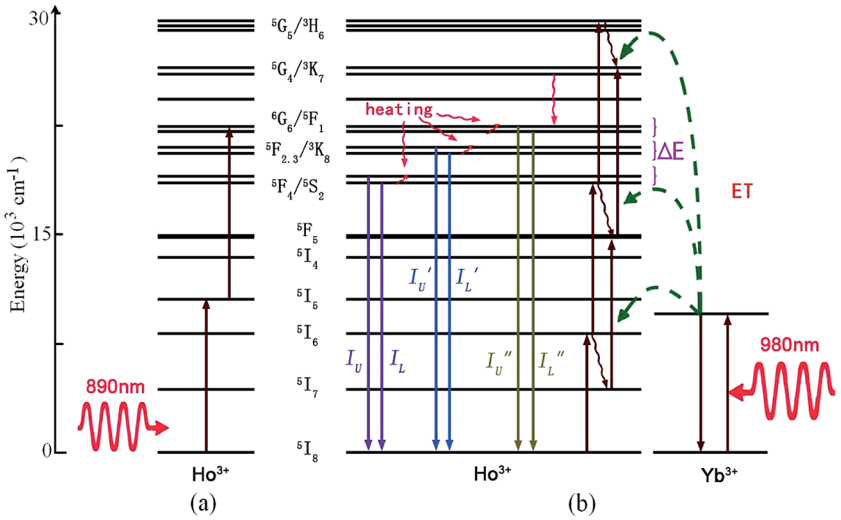

Fig. 9 The mechanism of optical thermal sensing through (a) up-conversion of the Ho^{3+} ion under 890 nm infrared excitation, and (b) Yb^{3+}–Ho^{3+} energy transfer under 980 nm infrared excitation.

luminescence intensity ratios, I_U/I_L and I_U'/I_L', change with the temperature of the phosphors. These temperature dependent fluorescence intensity ratios are used as the precise evaluation scale of optical temperature sensing.

Recently, based on down-conversion luminescence emissions centered at 524 nm ($^2H_{11/2} \rightarrow {}^4I_{15/2}$) and 547 nm ($^4S_{3/2} \rightarrow {}^4I_{15/2}$) of Er^{3+} ions, as shown in Fig. 4, optical temperature sensing in the range from 313 K to 713 K was studied by Sui *et al.* through analyzing the temperature dependent term R in Er^{3+} doped Te–Ge–Zn–Na glass under 379 nm excitation.[21] A maximum sensitivity of 0.0085 K^{-1} at 596 K was obtained in the $Te_{40}Ge_{40}Zn_{9.5}Na_{10}$ glass. Under 406 nm excitation, the intensity ratio of green emissions at 523 nm and 545 nm was studied by González *et al.* in Er^{3+} doped fluoroindate glass with a maximum sensitivity of 0.0028 K^{-1} for 425 K.[22] Under 488 nm excitation, the thermalized levels $^4S_{3/2}$ and $^2H_{11/2}$ were studied in Er^{3+} doped $NaYF_4$ nanocrystalline glass ceramic with a maximum sensitivity of 66 × 10^{-4} K^{-1} for 570 K.[23] Similarly, the maximum sensitivity of 79 × 10^{-4} K^{-1} for 630 K was obtained in Er^{3+} doped zinc fluorophosphate glass, and 79 × 10^{-4} K^{-1} for 541 K was obtained in Er^{3+} doped fluorotellurite glass.[24,25] Under 532 nm excitation, González *et al.*

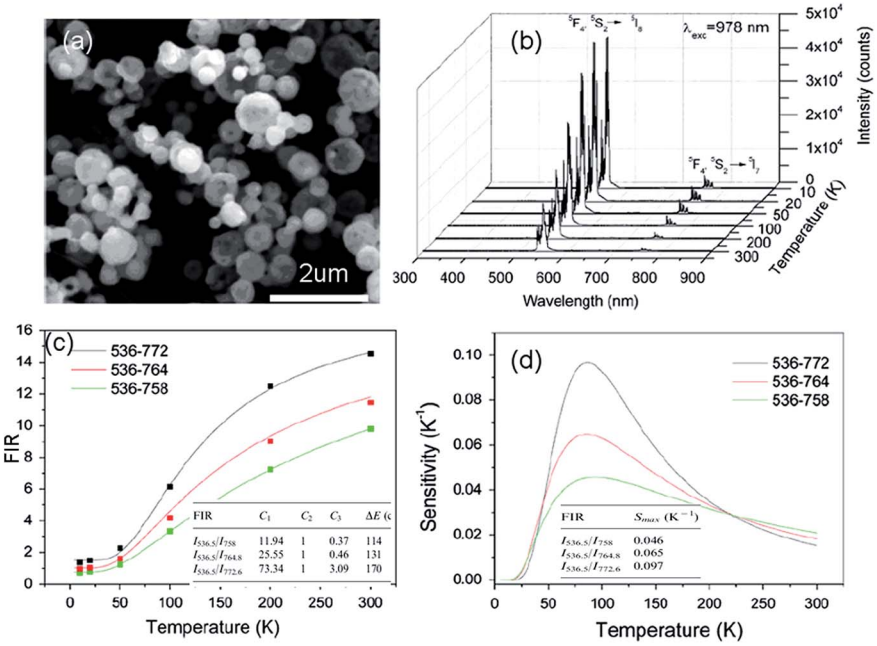

Fig. 10 (a) SEM image, (b) up-conversion spectra under 978 nm excitation, (c) FIR of emission at 536 nm relative to 758 nm, 764 nm and 772 nm emissions, and (d) the temperature dependence of sensitivity of Y_2O_3:Yb^{3+}, Ho^{3+} particles. Reproduced from ref. 59 with permission of Elsevier.

Table 4 The maximum sensitivity values of Ho^{3+} doped phosphors by the fluorescence intensity ratio technique are presented, and the involved transitions from the TCL, excition wavelength, emission wavelength, and temperature range are included

Rare-earth ions	Host	λ_{ex} (nm)	λ_{em} (nm)	Transitions	Temperature range (K)	S_R (maximum)	S_A	Ref.
Ho^{3+}	In–Zn–Sr–Ba glass	473	545, 750	$^5F_4/^5S_2 \rightarrow {}^5I_8, {}^5I_7$	20–300	0.0036 K^{-1} (59 K)	$181.64/T^2$	22
Ho^{3+}	TeO_2 glass	890	538, 545	$^5F_4, {}^5S_2 \rightarrow {}^5I_8$	265–440	0.0098 K^{-1} (130 K)	$255/T^2$	62
Ho^{3+}	$LiTeO_2$ glass	890	538, 543	$^5F_4, {}^5S_2 \rightarrow {}^5I_8$	265–383	0.0063 K^{-1} (265 K)	$255/T^2$	63
Ho^{3+}, Yb^{3+}	Y_2O_3	978	536.5, 772.6	$^5F_4/^5S_2 \rightarrow {}^5I_8, {}^5I_7$	10–300	0.0097 K^{-1} (85 K)	$241.2/T^2$	60
Ho^{3+}, Yb^{3+}	$Ba_{0.77}Ca_{0.23}TiO_3$	980	546, 754	$^5F_4/^5S_2 \rightarrow {}^5I_8, {}^5I_7$	93–300	0.0053 K^{-1} (93 K)	$182.3/T^2$	64
Ho^{3+}, Yb^{3+}	$Ca_{12}Al_{14}O_{33}$	980	467, 492, 542, 552	$^5G_4/^5G_5, {}^5F_4/^5S_2 \rightarrow {}^5I_8$	298–500			65
Ho^{3+}, Yb^{3+}	$CaMoO_4$	980	460, 489	$^5F_3, {}^3K_8 \rightarrow {}^5I_8$	303–543	0.0066 K^{-1} (353 K)	$648.5/T^2$	66
Ho^{3+}, Yb^{3+}	$CaWO_4$	980	460, 487	$^5G_6/^5F_1, {}^5F_{2,3}/^3K_8 \rightarrow {}^5I_8$	303–923	0.0050 K^{-1} (923 K)	$1890/T^2$	67
Ho^{3+}, Yb^{3+}	PbF_2 glass ceramic	980	445, 485	$^5G_6/^5F_1, {}^5F_{2,3}/^3K_8 \rightarrow {}^5I_8$	303–643	0.00102 K^{-1} (1119 K)	$2191.9/T^2$	68

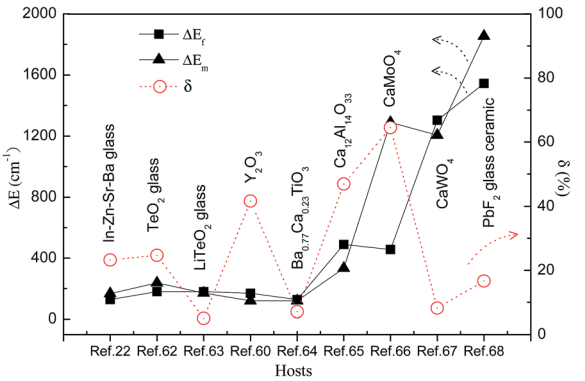

Fig. 11 Host dependent ΔE_f and ΔE_m between the TCL of Ho^{3+} ions, and the corresponding δ values.

demonstrated novel optical temperature thermometry based on infrared emissions centered at 800 nm ($^2H_{11/2} \rightarrow {}^4I_{13/2}$) and 850 nm ($^4S_{3/2} \rightarrow {}^4I_{13/2}$) in Er^{3+} doped Sr–Ba–Nb–B glass ceramic.[26] A maximum sensitivity of 0.0017 K^{-1} for 600 K was obtained. The hosts, excitation wavelength (λ_{ex}), emission wavelength (λ_{em}), the involved transitions, S_R and S_A values, and the temperature range for phosphors doped with Er^{3+} ions are summarized in Table 1.

(2) Up-conversion of Er^{3+} ions under infrared excitation: under infrared excitation, the excited states of Er^{3+} ions are populated by the GSA and successive excited state absorption (ESA),[27–36] as shown in Fig. 3(b). It needs three 1540 nm infrared photons and two 800 nm (or 980 nm) infrared photons to populate the thermally coupled $^2H_{11/2}$ and $^4S_{3/2}$ energy levels. The energy transfer between Er^{3+} ions is thought of as the main up-conversion mechanism, only when the Er^{3+} concentration of the optically active center is high enough.[13] The ions in the high energy excited states relax to the next lower energy levels $^2H_{11/2}$ and $^4S_{3/2}$ through non-radiative relaxation, giving two green emissions with the intensities of I_U and I_L. The temperature dependent fluorescence intensity ratio, I_U/I_L, is used as the precise evaluation scale of optical temperature sensing.

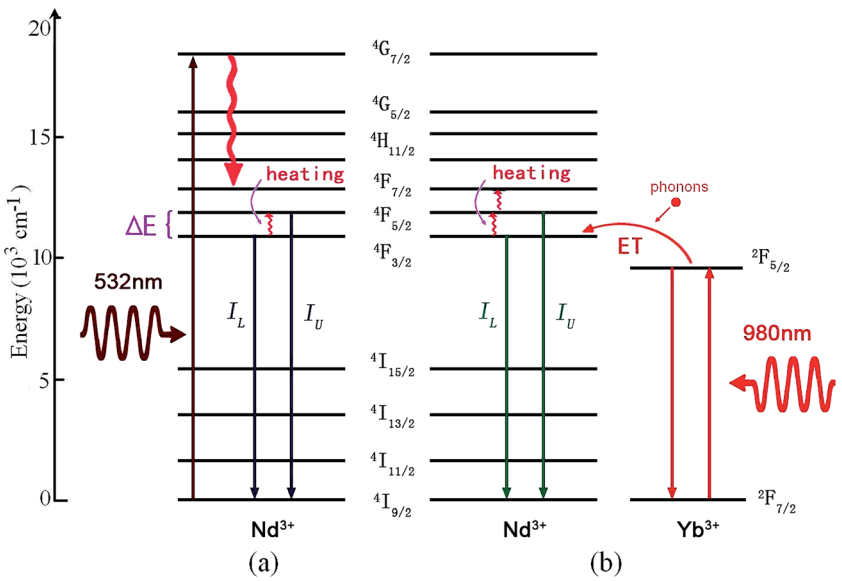

Fig. 12 The mechanism of optical thermal sensing through (1) down-conversion of the Nd^{3+} ion under 532 nm green excitation, and (2) Yb^{3+}–Nd^{3+} energy transfer under 980 nm infrared excitation.

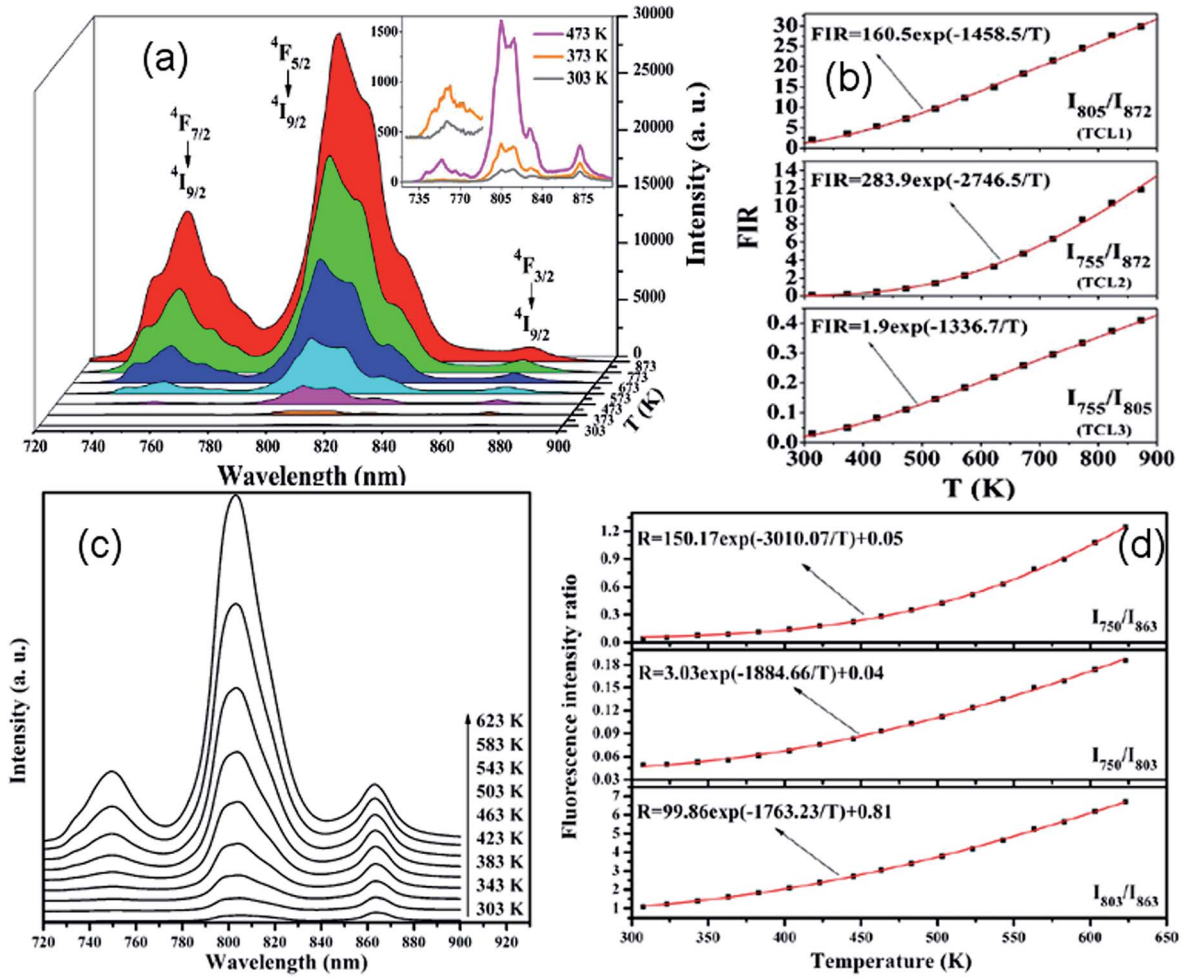

Fig. 13 Temperature dependent (a) near infrared emission spectra and (b) fluorescence intensity ratio (FIR) in Nd^{3+}/Yb^{3+} co-doped $CaWO_4$ phosphors excited by a 980 nm laser. Temperature dependent (c) near infrared emission spectra and (d) FIR in Nd^{3+}/Yb^{3+} co-doped oxyfluoride glass ceramic containing PbF_2 nanocrystals excited by a 980 nm laser. Reproduced from ref. 70 and 71 with permission of Optical Society of America and Elsevier.

Based on the up-conversion luminescence emissions centered at 524 nm ($^2H_{11/2} \rightarrow {}^4I_{15/2}$) and 547 nm ($^4S_{3/2} \rightarrow {}^4I_{15/2}$) of Er^{3+} ions, the optical temperature thermometry was studied by Luis *et al.* in a fluorotellurite glass under 800 nm excitation.[27] A better behaviour as a temperature sensor has been obtained for the less Er^{3+} concentrated glass with a maximum sensitivity of 54×10^{-4} K^{-1} at 540 K. Based on the thermalization effects between the upper levels responsible for green fluorescence at 522 nm and 546 nm under 805 nm laser excitation, new optical temperature sensing using the micrometer sized ZBLALiP spherical cavity was explored by Cai *et al.*[28] Using a diode laser emitting at about 980 nm as the excitation source, the optical temperature sensing properties based on green emissions of Er^{3+} ions were studies in BZT-BCT ferroelectric ceramics,

Table 5 The maximum sensitivity values of Nd^{3+} doped phosphors by the fluorescence intensity ratio technique are presented, and the involved transitions from the TCL, excition wavelength, emission wavelength, and temperature range are included

Rare-earth ions	Host	λ_{ex} (nm)	λ_{em} (nm)	Transitions	Temperature range (K)	S_R (maximum)	S_A	Ref.
Nd^{3+}	P–K–Ba–Al glass	532	810, 880	$^4F_{5/2}$, $^4F_{3/2} \rightarrow {}^4I_{9/2}$	300–850	0.0153 K^{-1} (300 K)	$1306.47/T^2$	69
Nd^{3+}, Yb^{3+}	$CaWO_4$	980	755, 872	$^4F_{7/2}$, $^4F_{3/2} \rightarrow {}^4I_{9/2}$	303–873		$2746.5/T^2$	70
			805, 872	$^4F_{5/2}$, $^4F_{3/2} \rightarrow {}^4I_{9/2}$			$1458.5/T^2$	
			755, 805	$^4F_{7/2}$, $^4F_{5/2} \rightarrow {}^4I_{9/2}$			$1336.7/T^2$	
Nd^{3+}, Yb^{3+}	PbF_2 glass	980	750, 863	$^4F_{7/2}/{}^4S_{3/2}$, $^4F_{3/2} \rightarrow {}^4I_{9/2}$	303–623		$3010.07/T^2$	71
	Ceramic		750, 803	$^4F_{7/2}/{}^4S_{3/2}$, $^2H_{9/2}/{}^4F_{5/2} \rightarrow {}^4I_{9/2}$			$1884.66/T^2$	
			803, 863	$F_{5/2}/{}^2H_{9/2}$, $^4F_{3/2} \rightarrow {}^4I_{9/2}$			$1763.23/T^2$	

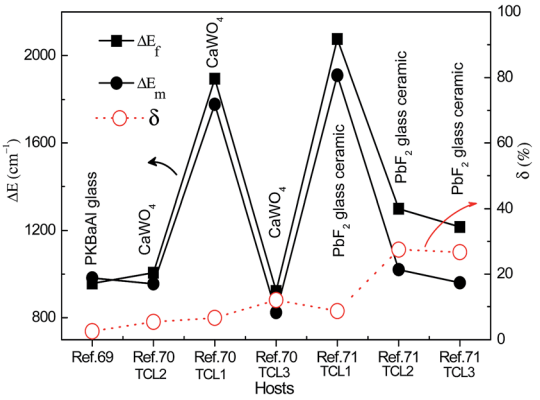

Fig. 14 Host dependent ΔE_f and ΔE_m between the TCL of Nd^{3+} ions, and the corresponding δ values.

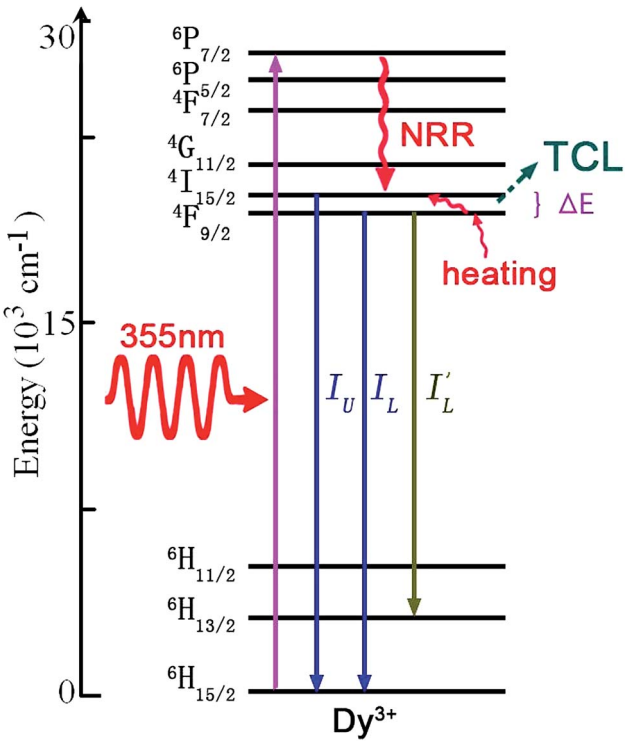

Fig. 15 The mechanism of optical thermal sensing through down-conversion of the Dy^{3+} ion under 355 nm ultraviolet excitation.

silicate glass, $BaTiO_3$ nanocrystals, PLZT transparent ceramics, $Yb_3Al_5O_{12}$ nanocrystals, and ZnO nanocrystals, respectively.[29–34] The maximum sensitivity of 48 × 10^{-4} K^{-1} for 467 K was obtained in Er^{3+} doped $Yb_3Al_5O_{12}$ nanocrystals. Under 1540 nm infrared excitation, based on green luminescence emissions of Er^{3+} ions, the optical temperature sensing properties were studied in Ga_2S_3–La_2O_3 chalcogenide glass, and the $Na_{0.82}Ca_{0.08}Er_{0.16}Y_{0.853}F_4$ phosphor.[35,36] The corresponding results are summarized in Table 1.

(3) Yb^{3+}–Er^{3+} energy transfer under infrared excitation: at high temperature, fluorescence quenching of emission bands of Er^{3+} ions induced by the temperature was obvious at 423 K.[21–35] It is necessary to enhance the emission intensity of phosphors in the process research of optical temperature sensing.

Among the rare-earth ions, the Yb^{3+} ion consists of only two levels, and has only one electronic excited state, $^2F_{5/2}$, that is located in the near infrared region at about 980 nm.[13] Moreover, high power InGaAs diode lasers are available to directly pump the Yb^{3+} absorption band around 980 nm. Fluorescent materials with Yb^{3+} as a sensitizer can convert short infrared into visible/ultraviolet light *via* energy transfer between lanthanide ions. As reported, the doping content of Yb^{3+} was usually kept at 18% or higher, because the large energy gap between the excited state $^2F_{5/2}$ and ground state $^2F_{7/2}$ blocks multiphoton cross-relaxation.[14] Thus, in order to enlarge the photo-absorption cross section of 980 nm infrared light, the Yb^{3+} ion is chosen to be a sensitizer for the Er^{3+} ion. Under 980 nm excitation, the two successive energy transfers from Yb^{3+} to Er^{3+} can induce the population of the thermally coupled $^2H_{11/2}$ and $^4S_{3/2}$ levels of Er^{3+},[37,39–50] and five successive energy transfers from Yb^{3+} to Er^{3+} can induce the population of the thermally coupled $^4D_{7/2}$ and $^4G_{9/2}$ levels of Er^{3+},[38] as shown in Fig. 3(c). The temperature dependent fluorescence intensity ratios, I_U/I_L and I'_U/I'_L, are used to evaluate the optical temperature sensing properties.

Recently, in the low temperature range, based on green luminescence emissions of Er^{3+}–Yb^{3+} co-doped $NaYF_4$ nanoparticles, Vetrone *et al.* demonstrated the optical temperature sensing properties in the internal temperature of the living HeLa cervical cancer cell from 25 °C to 45 °C.[37] Notably, the temperature dependence of the five-photon 256 nm ($^4D_{7/2}$ → $^4I_{15/2}$) and 276 nm ($^4G_{9/2}$ → $^4I_{15/2}$) ultraviolet up-conversion luminescence in Yb^{3+}–Er^{3+} co-doped β-NaLuF4 nanocrystals was studied firstly by Zheng *et al.* from 303 K to 523 K with a maximum sensitivity of 0.0052 K^{-1} at 303 K,[38] as shown in Fig. 5.

In the high temperature range, special phosphors are needed with high thermal stability and high solubility between hosts and lanthanide ions. Among the oxide materials, Y_2O_3 is a good candidate host, due to its wide bandgap, high melting point, high solubility between Y^{3+} and Er^{3+}, and good transparency from ultraviolet to infrared. Recently, in Er^{3+}–Yb^{3+} co-doped Y_2O_3 nanoparticles, optical temperature sensing properties were studied in the temperature range from 93 K to 613 K through analyzing the temperature dependent fluorescence intensity ratio of the two green emissions.[39–42] A maximum sensitivity of 528 × 10^{-4} K^{-1} for 150 K was obtained in the $Y_{1.97}Yb_{0.02}Er_{0.01}O_3$ nanophosphors.[40] The fluorescence intensity ratio of the green up-conversion emissions at 523 nm and 545 nm in Er^{3+}–Yb^{3+} co-doped Al_2O_3 was studied by Dong *et al.* as a function of temperature with a maximum sensitivity of 0.0051 K^{-1} at 495 K.[43] Additionally, oxide salts, such as $BaMoO_4$, Y_2SiO_5, MWO_4 (M = Ca, Sr), YVO_4, $BaTiO_3$, $Yb_2Ti_2O_7$, $Bi_7Ti_4NbO_{21}$, and $LiNbO_3$, were doped with Er^{3+} and Yb^{3+} ions, and were studied as optical temperature sensors by the temperature dependent fluorescence intensity ratio of the two green emissions.[43–54] From Table 1, one can find that the maximum S_R, 0.0528 K^{-1}, is obtained at 150 K in Er^{3+}–Yb^{3+} co-doped Y_2O_3 phosphors under 978 nm excitation, and the maximum S_A,

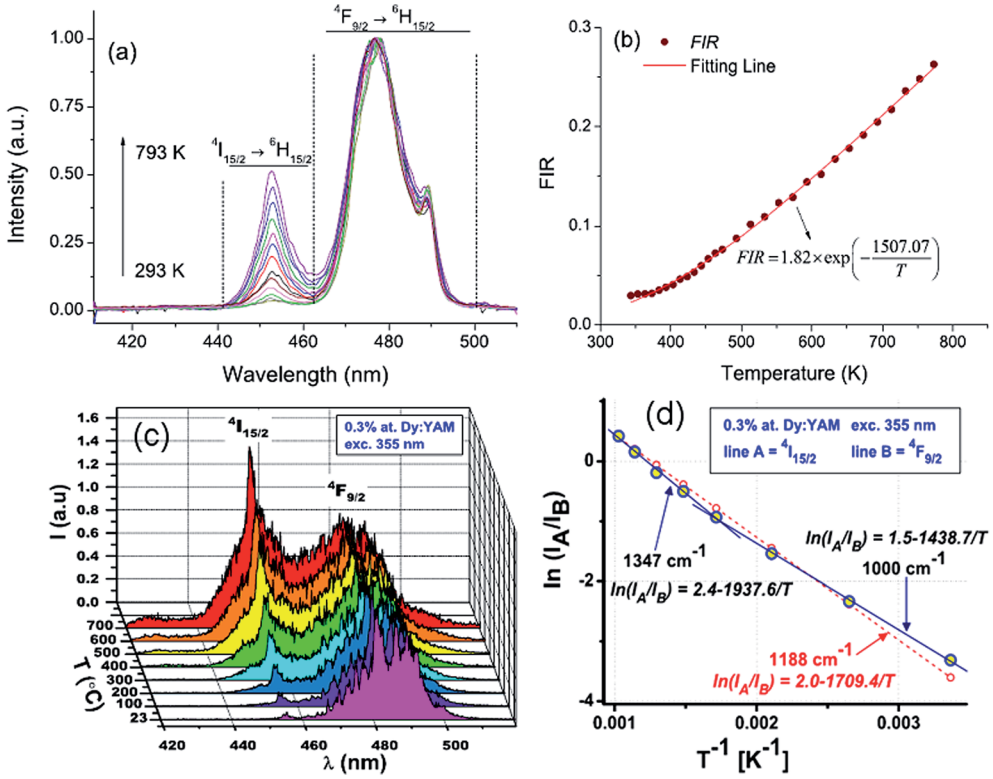

Fig. 16 Temperature dependent (a) emission spectra and (b) fluorescence intensity ratio (FIR) between the 455 nm and 478 nm emissions for the $BaYF_5$:2%Dy^{3+} sample. Temperature dependent (c) emission spectra and (d) Arrhenius plot of the intensity ratio for Dy^{3+} doped $Y_4Al_2O_9$ crystals. Reproduced from ref. 72 and 73 with permission of Optical Society of America and Elsevier.

$2109.31/T^2$, is obtained in Er^{3+}–Yb^{3+} co-doped $CaWO_3$ phosphors under 978 nm excitation.

The term δ is a key parameter used to judge the calculation accuracy of the fluorescence intensity ratio technique in the data fitting process. ΔE_f and ΔE_m between the TCL of Er^{3+} ions and the corresponding δ values are calculated and summarized in Table 2 through analyzing ref. 21–55. In Table 2, we can see that most of the Er^{3+} doped phosphors have a δ value of more than 5%, and the maximum δ value is about 53.89% for the Er^{3+} doped Si–B–Ba–Na glass. The δ values less than 5% are obtained in Er^{3+} doped tellurite glass, $Na_{0.82}Ca_{0.08}Er_{0.16}Y_{0.853}F_4$ bulks, PKAZLF glass, and ZBLALiP glass, respectively. The small δ values for tellurite, PKAZLF, and ZBLALiP glass materials can be explained as follows: the successive excited state absorption overcomes the energy transfer between the thermally coupled levels and other levels, due to the abnormal local ligand fields around the Er^{3+} sites in the tellurite, PKAZLF, and ZBLALiP glass hosts.[14,17] The population of the TCL of Er^{3+} ions at high temperature obeys the Boltzmann distribution. As shown in Table 2, most of the Er^{3+}–Yb^{3+} co-doped phosphors have a value of δ of more than 10%, and the maximum δ value is about 90% for the Er^{3+}–Yb^{3+} co-doped β-$NaLuF_4$ nanocrystals. Values of δ of less than 5% are observed in Er^{3+}–Yb^{3+} co-doped Y_2O_3, and Er^{3+}–Mo^{6+} co-doped $Yb_2Ti_2O_7$. The large δ value may be ascribed to the actual deviation of eqn (6) induced by energy transfer from the TCL to the other excited states.[14]

3.2 Optical thermometry based on Yb^{3+}–Tm^{3+} co-doped phosphors

The trivalent Tm^{3+} ion has a $4f^{12}$ electronic configuration, and is reported as one of the most efficient blue luminescence center ions. It has two couples of adjacent thermally coupled levels, such as $^3F_{2,3}$ and $^3H_4$, and $^1G_{4(a)}$ and $^1G_{4(b)}$, whose relative emission intensity is strongly temperature dependent. As

Table 6 The maximum sensitivity values of Dy^{3+} doped phosphors by the fluorescence intensity ratio technique are presented, and the involved transitions from the TCL, excition wavelength, emission wavelength, and temperature range are included

Rare-earth ions	Host	λ_{ex} (nm)	λ_{em} (nm)	Transitions	Temperature range (K)	S_R (maximum)	S_A	Ref.
Dy^{3+}	$BaYF_5$	355	455, 478	$^4I_{5/2}$, $^4F_{9/2} \rightarrow {}^6H_{15/2}$	293–773	0.02 K^{-1} (700 K)	$1507.07/T^2$	72
Dy^{3+}	$Y_4Al_2O_9$	355	455, 481	$^4I_{5/2}$, $^4F_{9/2} \rightarrow {}^6H_{15/2}$	296–573		$1438.7/T^2$	73
					573–973	0.003 $°C^{-1}$(973 K)	$1937.6/T^2$	

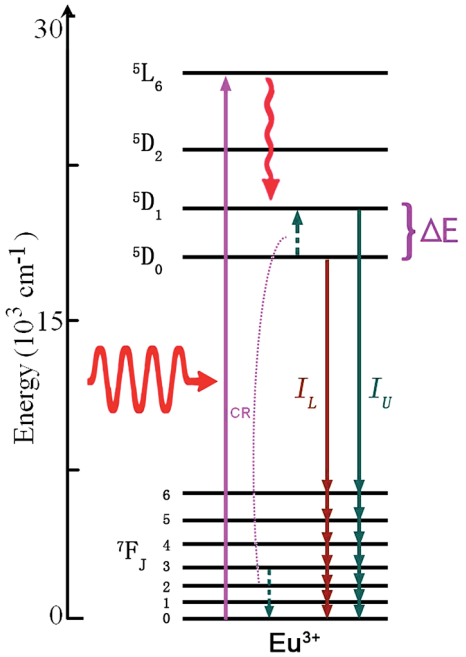

Fig. 17 The mechanism of optical thermal sensing through down-conversion of the Eu^{3+} ion under infrared excitation.

shown in Fig. 6, the energy transfer (ET) from Yb^{3+} to Tm^{3+} is the main population mechanism of optical thermometry based on up-conversion luminescence of the Tm^{3+} ion.[60] Under 980 nm infrared excitation, the thermally coupled levels $^1G_{4(a)}$ and $^1G_{4(b)}$ are populated by three successive ETs from Yb^{3+} to Tm^{3+}. The thermally coupled levels $^3F_{2,3}$ and $^3H_4$ are populated by two successive ETs from Yb^{3+} to Tm^{3+}. The ions in the high energy excited states, such as $^1G_{4(a)}$ and $^1G_{4(b)}$, $^3F_{2,3}$ and $^3H_4$, relax to the next lower energy levels through non-radiative relaxation, giving two blue emissions with the intensities I_U and I_L, and two infrared emissions with the intensities I'_U and I'_L. The temperature dependent fluorescence intensity ratios, I_U/I_L and I'_U/I'_L, are used to evaluate the optical temperature sensing properties.

The spectral properties of the Tm^{3+} luminescence band at 480 nm from the $^1G_4 \rightarrow {}^3H_6$ transition in Tm^{3+} and Yb^{3+} co-doped $NaNbO_3$ nanocrystals were analyzed in the biophysical temperature range from 297 K to 353 K with a 980 nm excitation source.[56] Novel TCL, $^1G_{4(a)}$ and $^1G_{4(b)}$, were observed firstly by Pereira *et al.* Experiments proved that the population redistribution among the thermally coupled stark levels could be successfully used for ratiometric thermal sensing. By analyzing the R value between the 700 nm and 800 nm up-conversion emissions, the optical temperature sensing properties of the Tm^{3+}/Yb^{3+} co-doped oxyfluoride PbF_2 glass ceramic were studied by Xu *et al.* in the temperature range of 293–703 K.[57] The optical

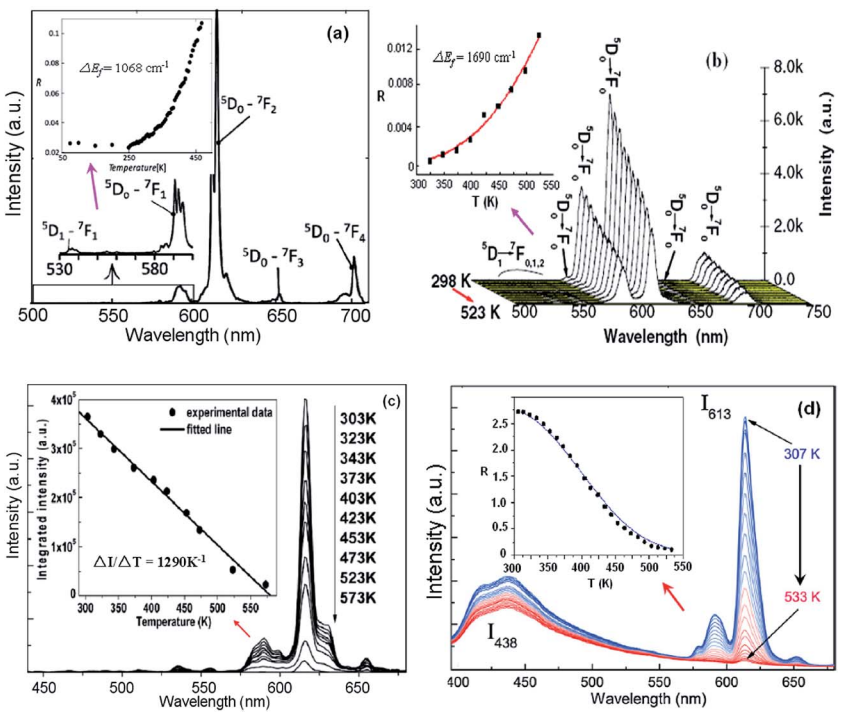

Fig. 18 (a) Emission spectrum of $CaGd_{1.8}Eu_{0.2}(WO_4)_4$ upon excitation at 395 nm. The inset is the integrated intensity ratio of the $^5D_1$ to $^5D_0$ emissions. (b) Temperature dependent emission spectra of $NaEuF_4$ spheres under 394 nm excitation. The inset is the emission intensity ratio of the $^5D_1$ to $^5D_0$ emissions with temperature. (c) Temperature dependent emission spectra of Sr_2CeO_4:Eu^{3+} under 365 nm excitation. The inset shows the integrated emission total intensity of 591 nm, 616 nm, and 654 nm at different temperatures. (d) Temperature dependent emission spectra of TiO_2:Eu^{3+} nanopowder. The inset is the emission intensity ratio of the 438 nm and 613 nm emissions with temperature. Reproduced from ref. 74–77 with permission of Optical Society of America and Elsevier.

Table 7 The maximum sensitivity values of Eu^{3+} doped phosphors by the fluorescence intensity ratio technique are presented, and the involved transitions from the TCL, excition wavelength, emission wavelength, and temperature range are included

Rare-earth ions	Host	λ_{ex} (nm)	λ_{em} (nm)	Transitions	Temperature range (K)	S_R (maximum)	S_A	Ref.
Eu^{3+}	$CaEu_2(WO_4)_4$ scheelite	395	535, 590	$^5D_1$, $^5D_0 \rightarrow {}^7F_1$	300–500	0.014 K^{-1} (300 K)	$1515.5/T^2$	77
Eu^{3+}	$NaEuF_4$ phosphor	394	500–560, 560–720	$^5D_1$, $^5D_0 \rightarrow {}^7F_1$	298–523	0.0043 K^{-1}	$2398.2/T^2$	78
Eu^{3+}	Sr_2CeO_4	365	591, 616, 654	$^5D_0 \rightarrow {}^7F_{1/2/3}$	303–573	1290 K^{-1}		79
Eu^{3+}	TiO_2 nanoparticles	360	438, 613	Host trap, $^5D_0 \rightarrow {}^7F_2$	307–533	0.0243 K^{-1} (533 K)		80

temperature sensing properties of Tm^{3+} were studied in Tm^{3+}–Yb^{3+} co-doped Y_2O_3 bulk and Y_2O_3 sub-micronic spherical particles.[58,59] The S_A and S_B values obtained from the Tm^{3+}–Yb^{3+} co-doped Y_2O_3 sub-micronic spherical particles are larger than those from the Tm^{3+}–Yb^{3+} co-doped Y_2O_3 bulk.

Recently, trivalent rare-earth ion doped fluoride nanocrystals were reported as the most efficient up-conversion materials.[13,14] Based on ultraviolet up-conversion emissions from the $^6P_{5/2}/^8S_{7/2}$ and $^6P_{7/2}/^8S_{7/2}$ TCL, Zheng *et al.* demonstrated firstly the optical temperature sensing properties in Tm^{3+}–Yb^{3+}–Gd^{3+} tri-doped $NaLuF_4$ microcrystals in the range of 298–523 K,[60] as shown in Fig. 7. The maximum sensor sensitivity of about 0.0029 K^{-1} was found at 298 K. The maximum sensor sensitivities were found to be about 0.0004 K^{-1} (333 K) and 0.0029 K^{-1} (298 K) by analyzing the ultraviolet emissions from the $^6P_{5/2}/^8S_{7/2}$ and $^6P_{7/2}/^8S_{7/2}$ levels, respectively. To our knowledge, fluoride nanocrystals are easily oxidized at high temperature. To overcome it, $NaYbF_4$:Tm^{3+}@SiO_2 core–shell materials were synthesized, and their optical temperature sensing properties based on the $^3F_2/^3H_4$ TCL of the Tm^{3+} ion were studied by Wang *et al.* in a wide temperature range from 100 K to 700 K.[61] A better behavior as a low temperature sensor has been obtained with a minimum sensitivity of 5.4×10^{-4} K^{-1} at 430 K.

In Table 3 we summarize, for the sake of comparison, the different performance parameters of sensitivities and the involved transitions of Tm^{3+} doped phosphors. The maximum value of S_R, 0.078 K^{-1}, is obtained in Tm^{3+}–Yb^{3+} co-doped Y_2O_3 sub-micronic spherical particles. The maximum value of S_A, $2829.5/T^2$, is obtained in Tm^{3+}/Yb^{3+} co-doped oxyfluoride PbF_2 glass ceramic. To study the feasibility evaluation in application, ΔE_f, ΔE_m, and δ are studied in Tm^{3+}–Yb^{3+} co-doped $NaNbO_3$ nanocrystals, oxyfluoride PbF_2 glass ceramic, Y_2O_3, $NaLuF_4$ microcrystals, and $NaYbF_4$ under 980 nm excitation, as shown in Fig. 8. A large δ value of more than 80% is observed in Tm^{3+}–Yb^{3+} co-doped $NaNbO_3$ nanocrystals. The large δ value may be ascribed to the actual deviation of eqn (6) induced by energy transfer from the TCL to the other excited states.[14] It is accurate to use $NaYbF_4$:Tm^{3+}@SiO_2 core–shell materials and Tm^{3+}/Yb^{3+} co-doped oxyfluoride Si–Pb glass ceramic to evaluate the scale of optical temperature sensing.

3.3 Optical thermometry based on Ho^{3+} doped phosphors

The trivalent Ho^{3+} ion has a $4f^{10}$ electronic configuration, and is reported as one of the most efficient green luminescence center ions, due to the intermediate $^5S_2$ level with a long fluorescence lifetime.[13,14] It has three couples of adjacent TCL, such as $^5F_4/^5S_2$, $^5F_{2,3}/^3K_8$, and $^5G_6/^5F_1$. As shown in Fig. 9, the two-step up-conversion of Ho^{3+} and successive energy transfer from Yb^{3+} to Ho^{3+} are the main mechanisms of optical thermometry based on Ho^{3+} doped phosphors.[60–68] In the case of a low doping concentration (<1%), the ESA process refers to a sequential absorption of two pump infrared photons at 890 nm by a single Ho^{3+} ion. Upon 980 nm laser irradiation, Yb^{3+} absorbs infrared photons with the generation of $^2F_{7/2} \rightarrow {}^2F_{5/2}$ upward transitions. Subsequently, it donates the energy to the adjacent Ho^{3+} through a phonon assisted energy transfer, with Yb^{3+} dropping back to its $^2F_{7/2}$ ground state. This promotes the Ho^{3+} ions to their excited states, such as $^5I_6$, $^5S_2$, and $^5G_5$. The thermally coupled $^5F_4/^5S_2$, $^5F_{2,3}/^3K_8$, and $^5G_6/^5F_1$ energy levels are populated by the process of non-radiative relaxation. The fluorescence intensity ratios, I_U/I_L, I'_U/I'_L, and I''_U/I''_L, are dependent strongly on temperature, and are used to study the optical temperature sensing properties.

It was reported that there were two formulas used to fit ΔE_f of the Ho^{3+} ions, due to the two different transitions, such as from the TCL to the other excited state, and from the TCL to the ground state. One formula is eqn (6), which is suitable to fit ΔE_f corresponding to transitions from $^5F_4/^5S_2$, $^5F_{2,3}/^3K_8$, and $^5G_6/^5F_1$ to the $^5I_8$ ground state. Using eqn (6) as a fitting formula, the temperature dependent fluorescence intensity ratios were studied in Ho^{3+} doped TeO_2 glass and $LiTeO_2$ glass under 890 nm excitation,[62,63] and Ho^{3+}–Yb^{3+} co-doped $CaMoO_4$, $CaWO_4$, and PbF_2 glass ceramic under 980 nm excitation.[66–68] A maximum S_R of 0.098 K^{-1} for 130 K was obtained in Ho^{3+} doped TeO_2 glass, and a maximum S_A of $2191.9/T^2$ was obtained in Ho^{3+}–Yb^{3+} co-doped glass ceramic.

The other formula is as follows:

$$R_1 = \frac{1 + C_1 \exp(-\Delta E_f/KT)}{C_2 + C_3 \exp(-\Delta E_f/KT)} \quad (11)$$

where C_1, C_2 and C_3 are constants that depend on spontaneous emission rates, degeneracy of the energy levels and emission energies.[60] Eqn (11) is used to fit ΔE_f originating from the transitions of $^5F_4 \rightarrow {}^5I_8$ and $^5S_2 \rightarrow {}^5I_7$. Using eqn (11) as a fitting formula, the temperature dependent fluorescence intensity ratios were studied in Ho^{3+} doped In–Zn–Sr–Ba glass under 473 nm excitation,[22] Ho^{3+}–Yb^{3+} co-doped Y_2O_3 under 978 nm excitation,[60] and $Ba_{0.77}Ca_{0.23}TiO_3$ and $Ca_{12}Al_{14}O_{33}$ under 980 nm excitation.[64,65] The Ho^{3+}–Yb^{3+} co-doped Y_2O_3 powder was

obtained *via* the spray pyrolysis method; its SEM image in Fig. 10(a) shows that the resulting particles were spherical, submicronic in size and un-agglomerated. The up-conversion emission spectra in Fig. 10(b) show that the green (536 nm) and infrared (758, 764, and 772 nm) emissions were dependent strongly on temperature. Fig. 10(c) shows the experimental fluorescence intensity ratio (FIR) of emission at 536 nm relative to the emissions at 758 nm, 764 nm and 772 nm, and these were fitted with eqn (11). At temperatures of 85, 84 and 90 K, the sensitivity of Ho^{3+} in Fig. 10(d) exhibits maximum values of 0.097, 0.065 and 0.046 K^{-1} for emissions at 536/772, 536/764 and 536/758 nm, respectively. The values of fitted ΔE in the inset of Fig. 10(c) and sensitivity are dependent strongly on the FIR.

In Table 4 we summarize, for the sake of comparison, the different performance parameters of Ho^{3+} doped and Ho^{3+}–Yb^{3+} co-doped phosphors. The maximum value of S_R, 0.0098 K^{-1}, is obtained in Ho^{3+}–Yb^{3+} co-doped TeO_2 glass. The maximum value of S_A, 2191.9/T^2, is obtained in the Tm^{3+}/Yb^{3+} co-doped oxyfluoride PbF_2 glass ceramic.

To value the fitting accuracy, ΔE_f and ΔE_m between the TCL of the Ho^{3+} ions and the corresponding δ values are calculated in Fig. 11 through analyzing ref. 22, 60 and 62–68. The thermally coupled $^5F_4$/$^5S_2$ energy levels were studied as a temperature function in ref. 22, 60 and 62–65. The minimum δ value of 5.09% is obtained in Ho^{3+} doped $LiTeO_2$ glass. The thermally coupled $^5F_{2,3}$/$^3K_8$ energy levels were studied as a temperature function in ref. 66. A large δ value of 64.6% was obtained in Ho^{3+}–Yb^{3+} co-doped $CaMoO_4$. The thermally coupled $^5G_6$/$^5F_1$ energy levels were studied in ref. 67 and 68. A small δ value of 8.2% was obtained in Ho^{3+}–Yb^{3+} co-doped $CaWO_4$. The large δ value may be ascribed to the lack of correction on eqn (11). If eqn (11) is used directly to fit ΔE_f, energy transfers from the TCL to the other excited states will be neglected. In fact, when the Ho^{3+} concentration is high enough, the cross-relaxation process, $^5S_2 + {}^5I_8 \rightarrow {}^5I_4 + {}^5I_7$, occurs frequently among Ho^{3+} ions.[13]

3.4 Optical thermometry based on Nd^{3+} doped phosphors

Among the rare-earth ions, Nd^{3+} has a $4f^3$ electronic configuration, and is reported as one of the most efficient activated ions to obtain laser emissions. It is significant work to study the optical thermal sensing of Nd^{3+} doped phosphors, since the temperature of the laser crystals can be monitored through analyzing the temperature dependent spectrum of Nd^{3+}. Nd^{3+} has three couples of adjacent thermally coupled levels, $^4F_{5/2}$/$^4F_{3/2}$ (TCL1), $^4F_{7/2}$/$^4F_{3/2}$ (TCL2), and $^4F_{7/2}$/$^4F_{5/2}$ (TCL3). As shown in Fig. 12, the mechanism of optical thermometry of Nd^{3+} doped phosphors is up-conversion and energy transfer from Yb^{3+} to Nd^{3+} assisted with phonons.[69–71] It needs one 532 nm green photon to populate the thermally coupled $^4F_{5/2}$ and $^4F_{3/2}$ energy levels through non-radiative relaxation. Upon 980 nm laser irradiation, Yb^{3+} absorbs infrared photons with the generation of $^2F_{7/2} \rightarrow {}^2F_{5/2}$ upward transitions. Subsequently, it donates the energy to the adjacent Nd^{3+} through a phonon assisted energy transfer, with Yb^{3+} dropping back to its $^2F_{7/2}$ ground state. This promotes the Nd^{3+} ions to their excited state, $^4F_{3/2}$. The $^4F_{5/2}$ energy level is populated by thermal excitation. The fluorescence intensity ratio, I_U/I_L, is dependent strongly on temperature, and is used to study the optical temperature sensing properties.

Recently, based on down-conversion luminescence emissions centered at 810 nm and 880 nm of Nd^{3+} ions, optical temperature sensing in the temperature range from 300 K to 850 K was studied by Rodríguez *et al.* in Nd^{3+} doped phosphate glass under 532 nm excitation.[69] Using a 980 nm diode laser as an excitation source, the temperature sensing properties based on the infrared luminescence emissions at 755 nm, 805 nm, and 872 nm of Nd^{3+}/Yb^{3+} co-doped $CaWO_4$ powders has been discussed by Xu *et al.* in the temperature range from 303 K to 873 K,[70] as shown in Fig. 13(a). Three TCL, such as TCL1, TCL2, and TCL3, were proven by using the fluorescence intensity ratio technique, as shown in Fig. 13(b). Similarly, the temperature sensing properties based on near infrared emissions from TCL1, TCL2, and TCL3 of Nd^{3+}/Yb^{3+} co-doped oxyfluoride glass ceramic containing PbF_2 nanocrystals were studied by Xu *et al.* as a function of temperature in the range of 303–623 K,[71] as shown in Fig. 13(c) and (d). In Table 5 we summarize, for the sake of comparison, the different performance parameters of Nd^{3+} doped and Nd^{3+}–Yb^{3+} co-doped phosphors.

The ΔE_f and ΔE_m values between the TCL of Nd^{3+} ions and the corresponding δ values are calculated in Fig. 14 through analyzing ref. 69–71. The temperature dependent emissions at 810 nm and 880 nm from TCL1 were studied in Nd^{3+} doped phosphate glass (ref. 69), and a small δ value of 2.55% was obtained. The temperature dependent emissions at 755 nm, 805 nm, and 872 nm from TCL1, TCL2, and TCL3 were studied in the Nd^{3+}–Yb^{3+} co-doped $CaWO_4$ powders (ref. 70). The δ values corresponding to TCL1, TCL2 and TCL3 are calculated to be 6.58%, 5.34%, and 12.03%. The temperature dependent emissions at 750 nm, 803 nm, and 863 nm from TCL1, TCL2, and TCL3 were studied in the Nd^{3+}–Yb^{3+} co-doped oxyfluoride glass ceramic (ref. 71). The corresponding δ values are calculated to be 8.69%, 27.45%, and 26.67%. If TCL1 and TCL3 are used to study the optical temperature sensing properties, we can get small and large δ values, respectively. It may be ascribed to the actual deviation of eqn (6) induced by the cross-relaxation process between the Nd^{3+} ions, $^4F_{7/2} + {}^4I_{9/2} \rightarrow {}^4F_{3/2} + {}^4I_{11/2}$.[13]

3.5 Optical thermometry based on Dy^{3+} doped phosphors

The Dy^{3+} ion with a $4f^9$ electronic configuration has a couple of adjacent TCL, $^4I_{5/2}$ and $^4F_{9/2}$. As shown in Fig. 15, the mechanism of optical thermometry based on luminescence of Dy^{3+} ions is down-conversion induced by ultraviolet excitation.[72,73] Under ultraviolet excitation, Dy^{3+} ions are excited directly to the higher excited states by the GSA transition. The ions in the excited states relax to the next lower energy level, $^4I_{5/2}$ and $^4F_{9/2}$, through non-radiative relaxation. Three emissions with the intensities I_U, I_L, and I'_L occur by the radiative transitions from $^4I_{5/2}$/$^4F_{9/2}$ to $^6H_{13/2}$ and $^6H_{15/2}$. The luminescence intensity ratios, I_U/I_L and I_U/I'_L, change with temperature, and are the precise evaluation scale of optical temperature sensing.

Optical temperature sensing of the Dy^{3+} doped $BaYF_5$ nanoparticles was studied by Cao *et al.* in the temperature range from 293 K to 773 K.[72] The temperature dependent fluorescence spectra of Dy^{3+} ions under excitation of a 355 nm laser in Fig. 16(a) show that the intensity of the 455 nm emission increased with a temperature increase, and the intensity of the 478 nm emission was independent of temperature. The temperature dependent luminescence intensity ratio of the 455 nm and 478 nm emissions was fitted in Fig. 16(b), in which the line fitted very well with the experimental data at a temperature higher than 380 K. By analyzing the temperature dependent 455 nm and 481 nm blue emissions, Boruc *et al.* demonstrated optical temperature sensing of Dy^{3+} doped $Y_4Al_2O_9$ crystals.[73] Temperature dependent emission spectra in Fig. 16(c) show that the intensity of the 455 nm emission increased with a temperature increase, and the intensity of the 481 nm emission decreased with a temperature increase. Temperature dependent luminescence intensity ratios of two blue emissions in Fig. 16(d) show different sensitivity values in two temperature ranges, such as 296 K < T < 573 K and 573 K < T < 973 K. The performance parameters of Dy^{3+} doped $BaYF_5$ and $Y_4Al_2O_9$ are summarized in Table 6. To value the fitting accuracy, ΔE_f and ΔE_m between the TCL of Dy^{3+} ions and the corresponding δ values are calculated through analyzing ref. 72 and 73. The δ value for the Dy^{3+} doped $BaYF_5$ nanoparticles is 1.09%. For the Dy^{3+} doped $Y_4Al_2O_9$ crystals, the δ value is 18.8% at the temperature range 296 K < T < 573 K, and it is 11.8% at the temperature range 573 K < T < 973 K. It is accurate to use the Dy^{3+} doped $BaYF_5$ nanoparticles to evaluate the scale of optical temperature sensing.

3.6 Optical thermometry based on Eu^{3+} doped phosphors

Among the rare-earth ions, Eu^{3+} has a $4f^6$ electronic configuration, and is reported as one of the most efficient activated ions to realize red emission in light emitting diodes (LEDs).[74–76] It is very significant to study optical thermal sensing of Eu^{3+} doped phosphors, since the temperature of LEDs can be monitored through analyzing the temperature dependent spectrum of Eu^{3+}. Eu^{3+} has a couple of adjacent thermally coupled levels, $^5D_1$ and $^5D_0$. As shown in Fig. 17, the mechanism of optical thermometry based on luminescence of the Eu^{3+} ion is down-conversion induced by ultraviolet excitation.[77–80] Under ultraviolet excitation, Eu^{3+} ions are excited directly to the higher excited states by the GSA transition, and then relax to the next lower energy levels, $^5D_1$ and $^5D_0$, through non-radiative relaxation. Two emissions with the intensity of I_U and I_L occur by the radiative transitions from $^5D_1/^5D_0$ to ^7F_J ($J = 0, 1, 2, 3, 4, 5, 6$). At high temperature, for high Eu^{3+} concentration doped phosphors, the increase in the $^5D_1$ emissions may be attributed to a thermally assisted cross-relaxation (CR) process with the involvement of two Eu^{3+} ions initially in the excited $^5D_0$ and the $^7F_3$ state.[77]

Meert *et al.* reported that the luminescence intensity ratios of the $^5D_1$ to $^5D_0$ emissions of the Eu^{3+} doped $CaEu_2(WO_4)_4$ scheelites changed in an exponential form with a temperature increase,[77] as shown in Fig. 18(a). The temperature dependent luminescence of spherical $NaEuF_4$ phosphors with different particle sizes was studied by Tian *et al.*[78] Fig. 18(b) shows the temperature dependent emission spectra of the $NaEuF_4$ spheres of 300 nm under 394 nm excitation. ΔE_f was calculated by fitting the temperature dependent emission intensity ratios of the $^5D_1/^5D_0$ emissions. The sensitivity values of the spherical $NaEuF_4$ phosphors decreased with the size increase from 100 nm to 700 nm, and a sensitivity up to 0.43% K^{-1} was achieved when the particle size was 100 nm. The temperature dependent luminescence spectrum of Sr_2CeO_4:Eu^{3+} was studied by Shi *et al.*, as shown in Fig. 18(c). The integrated luminescence total intensity of the $^5D_0$ emissions at 591 nm, 616 nm, and 654 nm showed a line change relation in the temperature range from 373 K to 573 K.[79] Luminescence temperature sensing was studied by Nikolić *et al.* in Eu^{3+} doped TiO_2 nanoparticles over a temperature range of 307–533 K.[80] The 438 nm blue emission associated with the trap emission of the TiO_2 host and the emission peak of the Eu^{3+} ions at 613 nm are observed in Fig. 18(d) under continuous excitation at a wavelength of 360 nm. The temperature dependent luminescence intensity ratio of the 438 nm and 613 nm emissions was suitable to be used for temperature sensing. In Table 7 we summarize, for the sake of comparison, the different performance parameters of Eu^{3+} doped phosphors.

To value the fitting accuracy, ΔE_f and ΔE_m between the TCL of the Eu^{3+} ions and the corresponding δ values are calculated through analyzing ref. 77 and 78. The δ value for the Eu^{3+} doped $CaEu_2(WO_4)_4$ scheelites is 38.7%, and the δ value for the spherical $NaEuF_4$ phosphors is 2.5%. As for the Eu^{3+} doped TiO_2 and Sr_2CeO_4, the values of δ are difficult to give, due to the incomplete data in ref. 76 and 77.

4. Conclusion and challenges

In summary, we have presented a detailed review of the Er^{3+}, Tm^{3+}, Ho^{3+}, Nd^{3+}, Dy^{3+}, and Eu^{3+} doped phosphors to date for the achievement of optical temperature sensing from the analysis of temperature dependent spectra. It has been shown that many phosphors with small δ values can be used as basic light emitting materials for optical thermometry. In the case of Er^{3+}, Tm^{3+}, Ho^{3+}, Nd^{3+}, and Dy^{3+} doped phosphors ($\Delta E_m \leq 900$ cm^{-1}) thermal equilibrium can be assumed because the population of the thermally coupled levels follows a Boltzmann distribution. Beyond this limit changes in the emission intensities are due to the effect of "coupling/decoupling" at higher or lower temperatures. As in the case of the Eu^{3+} doped phosphors, the $^5D_1$ and $^5D_0$ levels ($\Delta E_f \sim 1725$ cm^{-1}) are thermally decoupled at lower temperatures, with thermalization at higher temperatures. With the significant fundamental scientific and technological knowledge already accumulated by past research, optical thermometry represents an encouraging prospect in the development of new temperature sensors. However, from the point of view of application, many challenges remain in the areas of materials science and physical mechanisms.

One related challenge is the issue of trying to find novel phosphor materials that can be used as temperature sensors at temperatures greater than 500 °C (773 K). Luminescence of rare-

earth ion doped phosphors mentioned in this review is very weak at temperatures greater than 773 K, due to intense thermal quenching. It is difficult to measure temperature change in the range of more than 500 °C through the conventional optical temperature sensing technology. New phosphors with low thermal quenching rates and high luminescence efficiency should be synthesized cheaply. Instead of rare-earth ions, new luminescence centers with high luminescence intensity at high temperature (>773 K) may be excellent candidate activated ions in novel fluorescence sensors.

Another main challenge facing the field of optical thermometry is the lack of understanding of the physical mechanisms determining the transitions between the electronic levels of both the host lattice and the rare-earth ions. A theoretical model describing thermal population between the TCL in eqn (6) is suitable to be used in the data fitting process only in the cases without energy transfer. In fact, energy transfer between the host and the rare-earth ions becomes active at high temperature, and energy transfer among the rare-earth ions becomes active at a high doping concentration. Thus, the error values of ΔE_f for some phosphors mentioned in this review are large at more than 10%. In order to improve the calculation accuracy, a theoretical model describing the thermal population between the TCL in eqn (6) should be corrected for different phosphors. Additionally, the thermal affection of the excitation source should be considered in eqn (6).

Finally, we also believe that phosphor thermometry will be widely used in the future, not only for temperature detection in special environments, but also for some medical therapeutic equipment. In this sense, the development of phosphors with high thermal sensitivity and low thermal quenching of fluorescence will yield significant advances in the design of new optical temperature sensors. Colloidal phosphors with a random flightchain with biological tissues will be the target of innovation for disease diagnoses through the technology of optical temperature sensing.

Acknowledgements

This work was supported by National Natural Science Foundation of China (11404171, 11374162), Natural Science Youth Foundation of Jiangsu Province (BK20130865), the Six Categories of Summit Talents of Jiangsu Province of China (2014-XCL-021), and the Natural Science Foundation of the Jiangsu Higher Education Institutions of China (14KJB430020).

References

1 F. Vetrone, R. Naccache, A. Zamarrón, A. J. de la Fuente, F. S. Rodríguez, L. M. Maestro, E. M. Rodriguez, D. Jaque, J. Solé and J. A. Capobianco, *ACS Nano*, 2010, **4**, 3254–3258.
2 C. Gunawan, M. Lim, C. P. Marquis and R. Amal, *J. Mater. Chem. B*, 2014, **2**, 2060–2083.
3 W. J. Liu and B. Z. Yang, *Sens. Rev.*, 2007, **27**, 298–309.
4 D. Jaque and F. Vetrone, *Nanoscale*, 2012, **4**, 4301–4326.
5 C. D. S. Brites, P. P. Lima, N. J. O. Silva, A. M. An, V. S. Amaral, F. Palacio and L. D. Carlos, *Nanoscale*, 2012, **4**, 4799–4829.
6 N. Armaroli and V. Balzani, *Energy Environ. Sci.*, 2011, **4**, 3193–3222.
7 E. D. Larson, G. Fiorese, G. J. Liu, R. H. Williams, T. G. Kreutz and S. Consonni, *Energy Environ. Sci.*, 2010, **3**, 28–42.
8 M. E. Borges, M. C. A. Galván, P. Esparza, E. Medina, P. M. Zarza and J. L. G. Fierro, *Energy Environ. Sci.*, 2008, **1**, 364–369.
9 L. Guo, W. P. Dong and S. T. Zhang, *RSC Adv.*, 2014, **4**, 41956–41967.
10 L. M. Maestro, C. Jacinto, U. R. Silva, F. Vetrone, J. A. Capobianco, D. Jaque and J. G. Solé, *Small*, 2011, **7**, 1774–1778.
11 J. R. Lakowicz, I. Gryczynski, V. Bogdanov and J. Kusba, *J. Phys. Chem.*, 1994, **98**, 334–342.
12 P. Löw, B. Kim, N. Takama and C. Bergaud, *Small*, 2008, **4**, 908–914.
13 H. Dong, L.-D. Sun and C.-H. Yan, *Chem. Soc. Rev.*, 2015, **44**, 1608–1634.
14 F. Wang and X. G. Liu, *Chem. Soc. Rev.*, 2009, **38**, 976–989.
15 S. G. Xiao, X. L. Yang, Z. W. Liu and X. H. Yan, *J. Appl. Phys.*, 2004, **96**, 1360.
16 M. D. Shinn, W. A. Sibley, M. G. Drexhage and R. N. Brown, *Phys. Rev. B: Condens. Matter Mater. Phys.*, 1983, **27**, 6635–6648.
17 S. A. Wade, S. F. Collins and G. W. Baxter, *J. Appl. Phys.*, 2003, **94**, 4743–4756.
18 M. Quintanilla, E. Cantelar, F. Cusso, M. Villegas and A. C. Caballero, *Appl. Phys. Express*, 2001, **4**, 022601.
19 V. K. Rai, *Appl. Phys. B: Lasers Opt.*, 2007, **88**, 297–303.
20 S. F. L. Luis, U. R. R. Mendoza, E. Lalla and V. Lavín, *Sens. Actuators, B*, 2011, **158**, 208–213.
21 G. Z. Sui, X. P. Li, L. H. Cheng, J. S. Zhang, J. S. Sun, H. Y. Zhong, Y. Tian, S. B. Fu and B. J. Chen, *Appl. Phys. B: Lasers Opt.*, 2013, **110**, 471–476.
22 P. H. González, S. F. L. Luis, S. G. Pérez and I. R. Martín, *Mater. Res. Bull.*, 2011, **46**, 1051–1054.
23 S. F. L. Luis, U. R. R. Mendoza, P. H. González, I. R. Martín and V. Lavín, *Sens. Actuators, B*, 2012, **174**, 176–186.
24 N. Vijaya, P. Babu, V. Venkatramu, C. K. Jayasankar, S. F. L. Luis, U. R. R. Mendoza, I. R. Martín and V. Lavín, *Sens. Actuators, B*, 2013, **186**, 156–164.
25 S. F. L. Luis, U. R. R. Mendoza, I. R. Martín, E. Lalla and V. Lavín, *Sens. Actuators, B*, 2013, **176**, 1167–1175.
26 P. H. González, I. R. Martín, L. L. Martín, S. F. L. Luis, C. P. Rodríguez and V. Lavín, *Opt. Mater.*, 2011, **33**, 742–745.
27 S. F. L. Luis, U. R. R. Mendoza, E. Lalla and V. Lavín, *Sens. Actuators, B*, 2011, **158**, 208–213.
28 Z. P. Cai and H. Y. Xu, *Sens. Actuators, A*, 2003, **108**, 187–192.
29 P. Du, L. H. Luo, W. P. Li, Q. Y. Yue and H. B. Chen, *Appl. Phys. Lett.*, 2014, **104**, 152902.
30 C. R. Li, B. Dong, C. G. Ming and M. K. Lei, *Sensors*, 2007, **7**, 2652–2659.
31 M. A. R. C. Alencar, G. S. Maciel and C. B. de Araújo, *Appl. Phys. Lett.*, 2004, **84**, 4753–4755.
32 A. S. S. de Camargo, J. F. Possatto, L. A. O. Nunes, E. R. Botero, E. R. M. Andreeta, D. Garcia and J. A. Eiras, *Solid State Commun.*, 2006, **137**, 1–5.

33 B. Dong, B. S. Cao, Y. Y. He, Z. Liu, Z. P. Li and Z. Q. Feng, *Adv. Mater.*, 2012, **24**, 1987–1993.
34 X. Wang, X. G. Kong, Y. Yu, Y. J. Sun and H. Zhang, *J. Phys. Chem. C*, 2007, **111**, 15119–15124.
35 P. V. dos Santos, M. T. de Araujo, A. S. Gouveia-Neto, J. A. M. Neto and A. S. B. Sombra, *IEEE J. Quantum Electron.*, 1999, **35**, 395–399.
36 X. F. Wang, C.-S. Liu and X. H. Yan, *RSC Adv.*, 2014, **4**, 24170–24175.
37 F. Vetrone, R. Naccache, A. Zamarrón, A. J. de la Fuente, F. S. Rodríguez, L. M. Maestro, E. M. Rodriguez, D. Jaque, J. G. Solé and J. A. Capobianco, *ACS Nano*, 2010, **4**, 3254–3258.
38 K. Z. Zheng, W. Y. Song, G. H. He, Z. Yuan and W. P. Qin, *Opt. Express*, 2015, **23**, 7653–7658.
39 V. K. Rai, A. Pandey and R. Dey, *J. Appl. Phys.*, 2013, **113**, 083104.
40 V. Lojpur, G. Nikoli and M. D. Dramianin, *J. Appl. Phys.*, 2014, **115**, 203106.
41 P. Du, L. H. Luo, Q. Y. Yue and W. P. Li, *Mater. Lett.*, 2015, **143**, 209–211.
42 R. Dey, A. Pandey and V. K. Rai, *Sens. Actuators, B*, 2014, **190**, 512–515.
43 B. Dong, D. P. Liu, X. J. Wang, T. Yang, S. M. Miao and C. R. Li, *Appl. Phys. Lett.*, 2007, **90**, 181117.
44 A. K. Soni, A. Kumari and V. K. Rai, *Sens. Actuators, B*, 2015, **216**, 64–71.
45 N. Rakov and G. S. Maciel, *Sens. Actuators, B*, 2012, **164**, 96–100.
46 N. Rakov and G. S. Maciel, *Opt. Lett.*, 2014, **39**, 3767–3769.
47 A. Pandey, V. K. Rai, V. Kumar, V. Kumar and H. C. Swart, *Sens. Actuators, B*, 2015, **209**, 352–358.
48 M. K. Mahata, K. Kumar and V. K. Rai, *Sens. Actuators, B*, 2015, **209**, 775–780.
49 P. Du and J. S. Yu, *Ceram. Int.*, 2015, **41**, 6710–6714.
50 P. Du, L. H. Luo, W. P. Li and Q. Y. Yue, *J. Appl. Phys.*, 2014, **116**, 014102.
51 W. Xu, Z. G. Zhang and W. W. Cao, *Opt. Lett.*, 2012, **37**, 4865–4867.
52 B. S. Cao, Y. Y. He, Z. Q. Feng, Y. S. Li and B. Dong, *Sens. Actuators, B*, 2011, **159**, 8–11.
53 H. Zou, J. Li, X. S. Wang, D. F. Peng, Y. X. Li and X. Yao, *Opt. Mater. Express*, 2014, **4**, 1545–1554.
54 M. Quintanilla, E. Cantelar, F. Cussó, M. Villegas and A. C. Caballero, *Appl. Phys. Express*, 2011, **4**, 022601.
55 A. Pandey, S. Som, V. Kumar, V. Kumar, K. Kumar, V. K. Rai and H. C. Swart, *Sens. Actuators, B*, 2014, **202**, 1305–1312.
56 A. F. Pereira, K. U. Kumar, W. F. Silva, W. Q. Santos, D. Jaque and C. Jacinto, *Sens. Actuators, B*, 2015, **213**, 65–71.
57 W. Xu, X. Y. Gao, L. J. Zheng, Z. G. Zhang and W. W. Cao, *Sens. Actuators, B*, 2012, **173**, 250–253.
58 D. Y. Li, Y. X. Wang, X. R. Zhang, K. Yang, L. Liu and Y. L. Song, *Opt. Commun.*, 2012, **285**, 1925–1928.
59 V. Lojpur, M. Nikolic, L. Mancic, O. Milosevic and M. D. Dramicanin, *Ceram. Int.*, 2013, **39**, 1129–1134.
60 K. Z. Zheng, Z. Y. Liu, C. J. Lv and W. P. Qin, *J. Mater. Chem. C*, 2013, **1**, 5502–5507.
61 X. F. Wang, J. Zheng, Y. Xuan and X. H. Yan, *Opt. Express*, 2013, **21**, 21596–21606.
62 A. K. Singh, *Sens. Actuators, A*, 2007, **136**, 173–177.
63 A. K. Singh and S. B. Rai, *Appl. Phys. B*, 2007, **86**, 661–666.
64 P. Du, L. H. Luo and J. S. Yu, *J. Alloys Compd.*, 2015, **632**, 73–77.
65 R. K. Verma and S. B. Rai, *J. Quant. Spectrosc. Radiat. Transfer*, 2012, **113**, 1594–1600.
66 R. Dey, A. Kumari, A. K. Soni and V. K. Rai, *Sens. Actuators, B*, 2015, **210**, 581–588.
67 W. Xu, H. Zhao, Y. X. Li, L. J. Zheng, Z. G. Zhang and W. W. Cao, *Sens. Actuators, B*, 2013, **188**, 1096–1100.
68 W. Xu, X. Y. Gao, L. J. Zheng, Z. G. Zhang and W. W. Cao, *Opt. Express*, 2012, **20**, 18127–18137.
69 C. P. Rodríguez, L. L. Martín, S. F. L. Luis, I. R. Martín, K. K. Kumar and C. K. Jayasankar, *Sens. Actuators, B*, 2014, **195**, 324–331.
70 W. Xu, Q. T. Song, L. J. Zheng, Z. G. Zhang and W. W. Cao, *Opt. Lett.*, 2014, **39**, 4635–4638.
71 W. Xu, H. Zhao, Z. G. Zhang and W. W. Cao, *Sens. Actuators, B*, 2013, **178**, 520–524.
72 Z. M. Cao, S. S. Zhou, G. C. Jiang, Y. H. Chen, C. K. Duan and M. Yin, *Curr. Appl. Phys.*, 2014, **14**, 1067–1071.
73 Z. Boruc, M. Kaczkan, B. Fetlinski, S. Turczynski and M. Malinowski, *Opt. Lett.*, 2012, **37**, 5214–5216.
74 D. Q. Chen, Y. L. Yu, P. Huang, H. Lin, Z. F. Shan and Y. S. Wang, *Acta Mater.*, 2010, **58**, 3035–3041.
75 S. H. Park, K. H. Lee, S. Unithrattil, H. S. Yoon, H. G. Jang and W. B. Im, *J. Phys. Chem. C*, 2012, **116**, 26850–26856.
76 J. Zhang, Y. M. Yang, Y. Z. Liu, C. Mi, G. Li, B. Han, Y. Zhang and H. J. Seo, *J. Am. Ceram. Soc.*, 2015, **98**, 1567–1573.
77 K. W. Meert, V. A. Morozov, A. M. Abakumov, J. Hadermann, D. Poelman and P. F. Smet, *Opt. Express*, 2014, **22**, 961–972.
78 Y. Tian, B. N. Tian, C. Cui, P. Huang, L. Wang and B. J. Chen, *Opt. Lett.*, 2014, **39**, 4164–4167.
79 L. L. Shi, C. Y. Li and Q. Su, *Opt. Lett.*, 2011, **36**, 582–584.
80 M. G. Nikolić, Ź. Antić, S. Ćulubrk, J. M. Nedeljković and M. D. Dramićanin, *Sens. Actuators, B*, 2014, **201**, 46–50.